

TNO report  
FEL-98-A077

## Geographical information extraction with remote sensing Part II of III - Technical Supplement

TNO Physics and Electronics  
Laboratory

**"DTIC USERS ONLY"**

Oude Waalsdorperweg 63  
PO Box 96864  
2509 JG The Hague  
The Netherlands

Phone +31 70 374 00 00  
Fax +31 70 328 09 61



All information which is classified according to Dutch regulations shall be treated by the recipient in the same way as classified information of corresponding value in his own country. No part of this information will be disclosed to any third party.

The classification designation Ongerubriceerd is equivalent to Unclassified, Stg. Confidencieel is equivalent to Confidential and Stg. Geheim is equivalent to Secret.

All rights reserved. No part of this report may be reproduced in any form by print, photoprint, microfilm or any other means without the previous written permission from TNO.

In case this report was drafted on instructions from the Ministry of Defence the rights and obligations of the principal and TNO are subject to the standard conditions for research and development instructions, established by the Ministry of Defence and TNO, if these conditions are declared applicable, or the relevant agreement concluded between the contracting parties.

© 1998 TNO

**DTIC QUALITY INSPECTED 1**

The TNO Physics and Electronics Laboratory is part of TNO Defence Research which further consists of:

TNO Prins Maurits Laboratory  
TNO Human Factors Research Institute

Date  
August 1998

Author(s)  
Dr A.C. van den Broek  
M. van Persie  
H.H.S. Noorbergen  
Dr G.J. Rijckenberg

Sponsor HWO-CO/HWO-KL  
Project officer J. Rogge  
Affiliation KMA

Classification  
Classified by J. Rogge  
Classification date 18 August 1998

Title Ongerubriceerd  
Report text Ongerubriceerd

Copy no 12  
No of copies 54  
No of pages 104 (excl distribution list)  
No of appendices -

19990126 151



AQF99-04-0711

Netherlands Organization for  
Applied Scientific Research (TNO)

## **REPRODUCTION QUALITY NOTICE**

**This document is the best quality available. The copy furnished to DTIC contained pages that may have the following quality problems:**

- **Pages smaller or larger than normal.**
- **Pages with background color or light colored printing.**
- **Pages with small type or poor printing; and or**
- **Pages with continuous tone material or color photographs.**

**Due to various output media available these conditions may or may not cause poor legibility in the microfiche or hardcopy output you receive.**

**If this block is checked, the copy furnished to DTIC contained pages with color printing, that when reproduced in Black and White, may change detail of the original copy.**

## Contents

Technical Supplement .....	3
S1. Sensors and image data .....	3
S1.1 Optical sensors and image data .....	9
S1.2 Thermal infrared sensors and image data .....	21
S1.3 Microwave sensors and image data .....	25
S2. Visualisation techniques .....	37
S2.1 False colour and simulated natural colour .....	37
S2.2 Combination of panchromatic and multi-spectral images .....	40
S2.3 Principal component analysis .....	42
S2.4 IHS transform and decorrelation stretch .....	44
S3. Extraction Techniques .....	47
S3.1 Terrain feature extraction .....	47
S3.2 Height determination .....	78
S3.3 Multitemporal analysis .....	94
S4. Sensor and data fusion .....	99

## Technical Supplement

### Geographical information extraction with remote sensing

#### S1. Sensors and image data

In this part of the report we give details about the sensors and platforms used. We furthermore describe extraction and visualisation techniques.

Imaging sensors operating in three wavelength regions are considered:

- optical/near-infrared
- thermal infrared
- microwave

The sensors are mounted on a so-called platform. We discriminate here between airborne and spaceborne platforms. Spaceborne platforms are always called satellites, while airborne platforms can be conventional aircrafts, but also UAV's, drones or even balloons. Main difference between space and airborne platforms is the distance between the sensor and the Earth surface, which ranges roughly from 100 km to 36,000 km for spaceborne and 10 meter to 20 km for airborne systems. The distance influences the information content of an image, especially the *resolution* and the *imaging geometry*.

We will discuss here the *resolution* and *imaging geometry* in a general context. In the next sections we will discuss for the three wavelength domains the following topics in more detail:

- physical background
- imaging geometry and image distortions
- present and future systems

#### *Resolution*

The resolution is a measure which determines the potential to observe details in an image. We discriminate here three different types of resolution:

1. **Spatial resolution:** the dimension on the ground of the smallest detail which can be seen in an image. This means that within a resolution cell no structure can be observed. An object smaller than the size of the resolution appears as a point in the image.
2. **Radiometric resolution:** the number of intensity levels, which are present in an image for a certain spectral band in the case of optical and thermal infrared sensors. For active microwave sensors radiometric resolution is sometimes referred to as the number of looks, which describes the amount of speckle in an image.

3. Spectral resolution: the number and width of spectral bands which the sensor can observe. This type of resolution is mainly applicable for hyperspectral scanners.

In general the spatial resolution for optical and thermal infrared systems is better when the distance is shorter. Optical spaceborne imagery from commercial satellites like SPOT has resolutions up to 10 m (in the near future 1 m optical imagery may be commercially obtainable), while camera's mounted on a UAV's or aeroplane can easily produce sub-dm images.

In principle the resolution for active microwave systems is independent of the distance. However due to the less favourable energy budget (higher spreading loss) for satellite systems, the spatial resolution is generally less than for airborne systems.

Presently spaceborne SAR's like the ERS SAR produce 25 m resolution imagery, while 1 m resolution is obtainable in spot light mode for dedicated (military) satellites. An airborne SAR may produce images with a resolution up to a few dm.

The concept *resolution* should not be confused with concepts like *pixel size* (pixel dimension) and *scale*.

- The pixel dimension is the size on the ground of an image element. In principle many pixels can cover a resolution element (oversampling). In order to restrict the data rate, the pixel size is usually chosen in the order of the resolution
- The scale of an image is only defined for a print out. This means that digital data is in principle not yet scaled, until a print out is made. Sometimes we deal with digitally scanned versions of maps or photographic plates. We then confusingly speak about the scale of the data, where we refer to the scale of the original map or photographic plate.

### *Imaging geometry*

The imaging geometry concerns the geometry between the sensor and the sensed surface and the way how the information is recorded. There are two main types of geometry:

1. radial type geometry
2. range type geometry

The first type of geometry is applicable to most optical and thermal infrared recordings, while the second type is applicable to microwave and lidar imaging. For simplicity we consider here recordings where one dimension is build due to the movement along the flying path (along track). In this way an imaging swath is created where the spatial resolution parallel to the flying path depends on the speed of the platform and the sampling frequency. The spatial dimension perpendicular to the flying path (across track) is created by varying the line of sight according to above mentioned geometries.

For the radial type geometry this is done by varying the angle between nadir and the line of sight.

This can be done by a rotating mirror or by an array of pixels in front of a lens (see section S1.1.1).

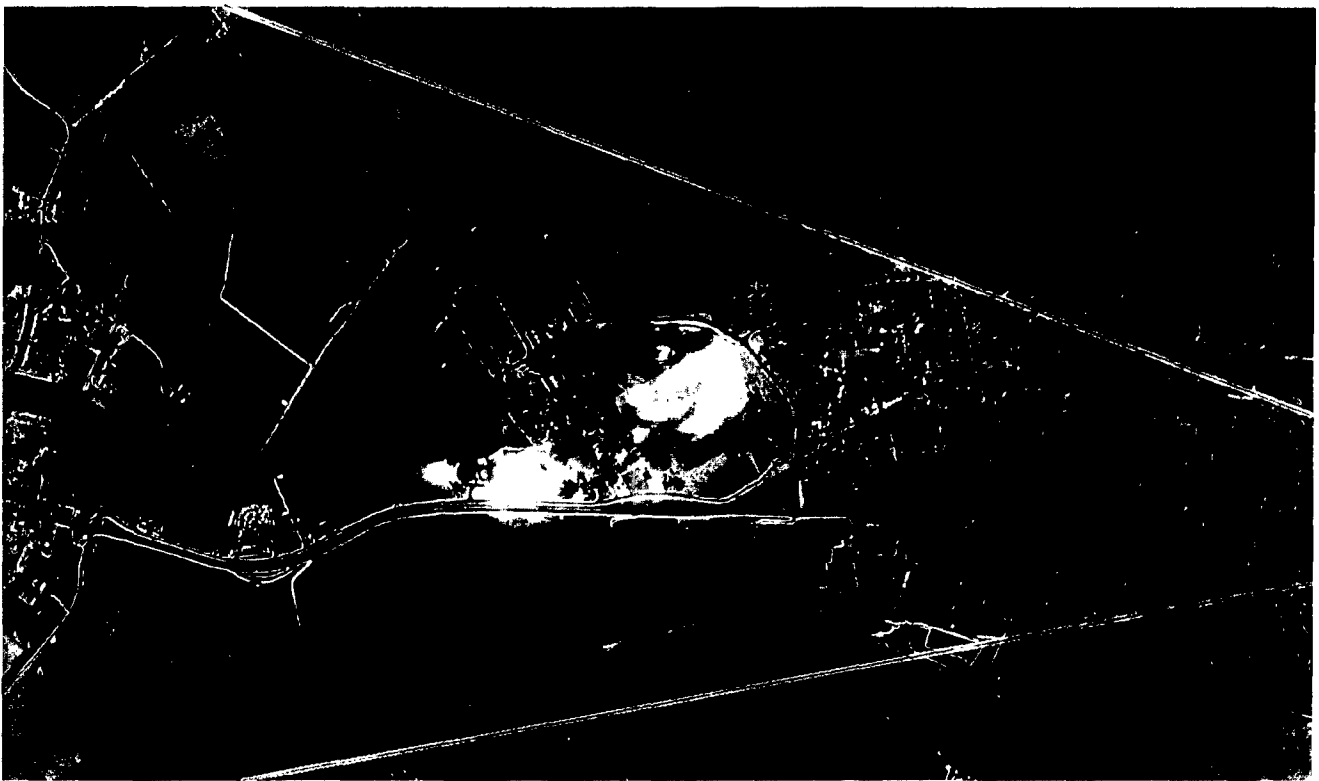
For the range type of geometry the across track dimension is build by sampling in time backscattered radiation from transmitted pulses. The delay between two recordings causes that the line of sight varies. This is only true when the angle between nadir and the line of sight differs significantly from zero.

Therefore microwave sensors need to be side-looking (i.e. a large look angle). Both geometry's cause that the across track resolution varies with the angle between the line of sight and nadir causing geometrical distortions (tangential scale distortions). The across track resolution varies for optical and thermal infrared sensors as

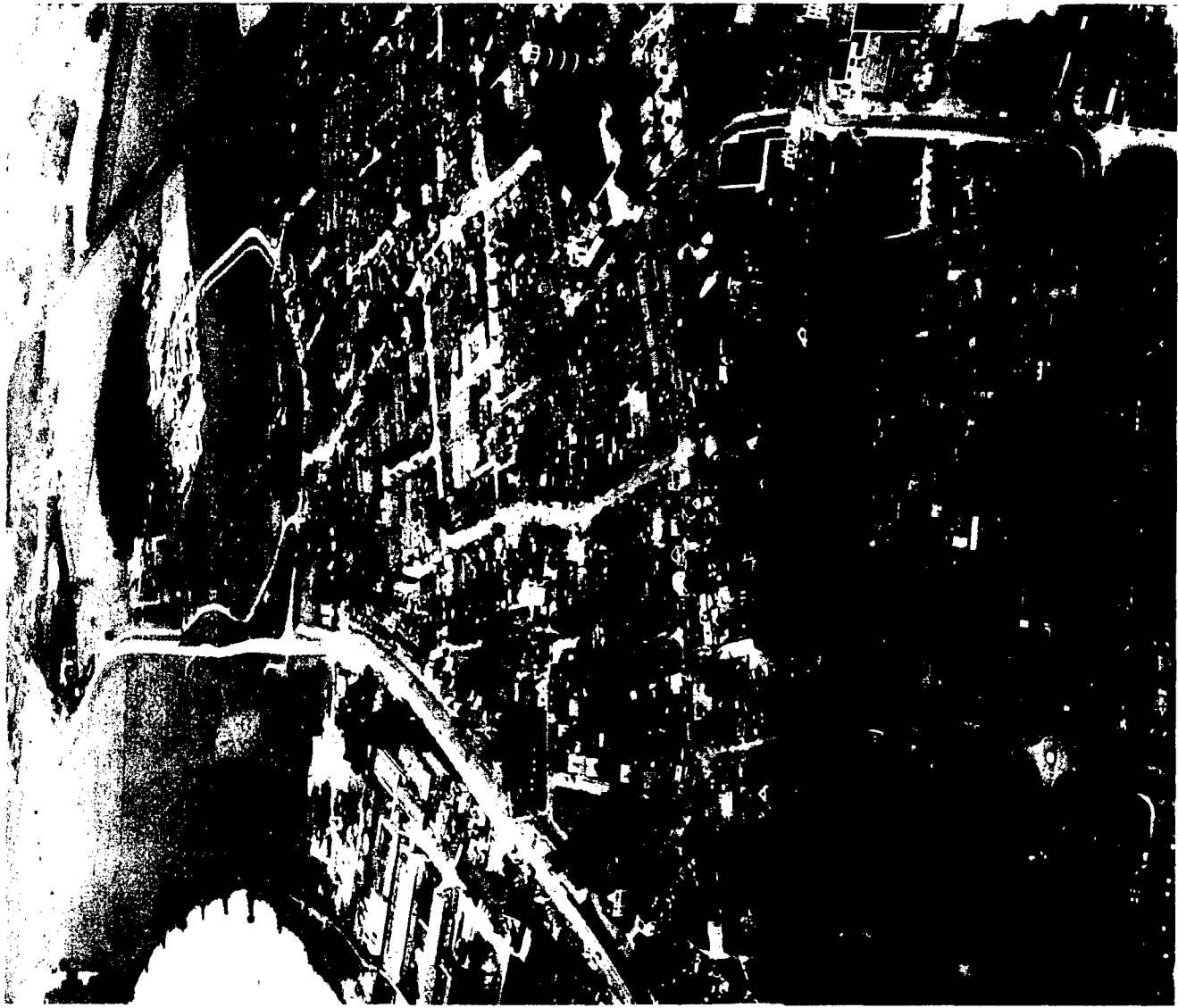
$$\rho_{\text{across}} = \rho_0 / \cos^2(\theta)$$

where  $\theta$  is the angle between nadir and the line of sight and  $\rho_0$  is the resolution at nadir ( $\theta = 0$ ; vertical viewing). In Figure S2 we exemplify this and also show the across resolution as function of  $\theta$ . From this Figure it is clear that severe geometrical distortions can be expected at the edges of the images when  $\theta$  is more than 45 degrees.

To exemplify this distortion we compare in Fig. S1 a CAESAR image (vertical viewing) with a SQ306 Orpheus image (extreme oblique viewing) near the village Olst. Clearly is seen that the buildings and forest patches to the top of the image are severely distorted in the Orpheus image compared to the CAESAR image. The yellow lines in the CAESAR image indicate the outline of the Orpheus image.



CAESAR (RGB: band 3,2,1)



SQ306 Orpheus image (oblique viewing)

Figure S1: Radial geometry distortion. See text for further explanation.

In the case of microwave imaging the across track resolution varies as

$$\rho_{\text{across}} = \rho_0 / \sin(\theta)$$

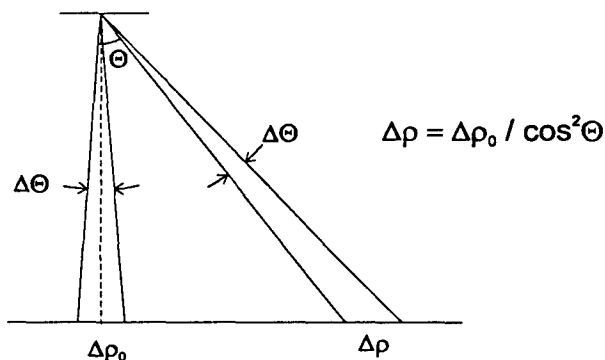
where  $\rho_0$  is now the resolution in the hypothetical situation that the radar is looking horizontal. i.e. the range resolution, which is 50% of the duration of the pulse. The distortion is now largest at near range for small  $\theta$ , as opposed to the situation in optical/thermal infrared recordings.

# Imaging geometry's

## Tangential scale distortion

### Radial type geometry

Optical and thermal infrared  
No distortion at  $\Theta = 0^\circ$



### Range type Geometry

Microwave  
No distortion at  $\Theta = 90^\circ$

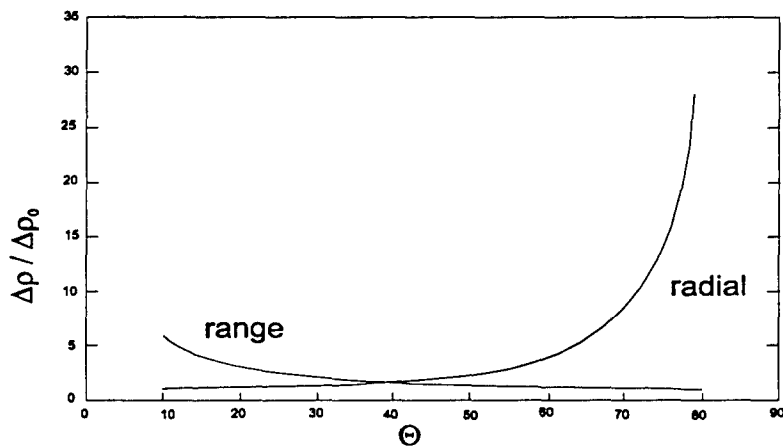
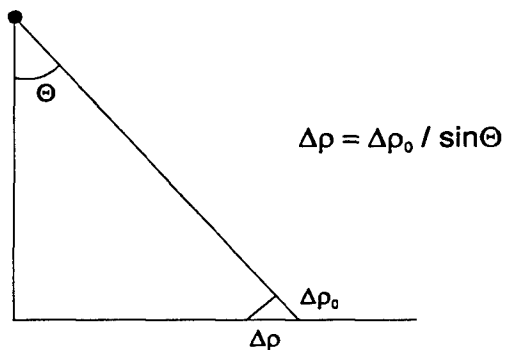


Figure S2: Tangential scale distortion for 'radial' and 'range' type geometries.

## **S1.1 Optical sensors and image data**

### **S1.1.1 Physical background**

#### **General**

Optical sensors can be characterised by a number of important features:

1. Optical sensors correspond to the human eye in many aspects. Most optical sensors make use of Silicon detectors which are sensitive in the spectral region of 400 to 1100 nanometer. The human eye is sensitive for light in the spectral region of 400 to 700 nanometer, corresponding to blue, green and red. The wavelengths of 700 to 1100 nanometer corresponds to the near-infrared part of the spectrum, where vegetation reflects strongly. Some sensors are also sensitive for the mid-infrared region of the spectrum, 1100 to 3000 nanometer, which contains information about vegetation and soil type.
2. Optical sensors can reach relatively high spatial resolutions. Resolutions of less than 0.5 meter from space and some centimetres from the air are possible. Limiting factors for the spatial resolution are the sensitivity of the detectors, the size of the lens or mirror and the refraction.
3. Optical sensors can only be used in daytime, since optical sensors make use of a natural light source, the Sun. So at night no observations are possible, and also for small solar incidence angles the observations are of low quality because of long shadows and low light intensities. Exceptions are lidars, which use laser as an active light source. The spatial resolution of these sensors is limited however.
4. Optical sensors are hindered by cloud cover. From an operational point of view this is an important limitation, since many parts of the world, including The Netherlands, are frequently covered by clouds. Optical observations from an aircraft or satellite are not possible for a thick layer of clouds. Also for thin high clouds or haze the quality of the images decreases severely.

Different types of optical sensors exist, which can be operated in several ways. We described them here.

#### **Sensor type**

1. Analogue sensor systems. These systems make use of continuous, in general conventional imaging mechanisms. The most clear example is the photocamera, by which the image is stored on photographic material. An advantage of this method is its relative simplicity, both for imaging and data storage. Disadvantages however are the difficult calibration, the limited radiometric and spectral resolution and the fact that the photographic material always should be sent physically to the earth (no transmission by an antenna is possible).
2. Digital systems. These systems make use of electronic observation. Advantage is the higher radiometric and spectral accuracy, the possibility to transmit the images to earth with a data-link and the possibility to automatically analyse the images. Disadvantage is the enormous amount of data.

3. A kind of mixture is formed by the video-cameras, whereby the analogue electronic signal is stored on tape and also can be transmitted to earth.

For the digital systems different mechanisms can be distinguished for imaging an area.

1. Rotating scanner. By this sensor mechanism there is only one sensor element per spectral channel. In order to build up a total image, the element scans the earth perpendicular to the flight direction by using a rotating mirror. As a consequence of the speed of the platform the image is built up in flight direction.
2. Pushbroom scanner. In this case the sensor consists of a long row of light sensitive elements (CCD's) with which in one moment a complete image line is observed. As a consequence of the speed of the platform the second image direction is built up.
3. Matrix-CCD sensors. These sensors do have a matrix of CCD-elements so that in one moment a complete image can be collected.

### **Spectral information**

Optical sensors can have a different number of spectral bands with a different bandwidth: We discriminate here between panchromatic, multi-spectral and hyperspectral sensors.

#### Panchromatic recordings

Panchromatic sensors. have only one, relative broad, spectral band, generally covering the region of 500 to 700 nm, resulting in a 'black and white' image, comparable with 'black and white' photographs. So the image contains little spectral (colour) information. The main reason why they are collected is that very high spatial resolutions can be reached because of the wide spectral band, collecting relatively much energy.

The philosophy behind panchromatic images is that the detection of light is always based on the detection of light-energy. The amount of light energy which is sensed depends on:

- The exposure time; the time-interval during which the energy is collected.
- The field of view; i.e. the area size from which the energy is collected.
- The spectral bandwidth which is used; the wider the spectral band, the more energy can be collected.
- The brightness of the optical system.

For obtaining maximum spatial resolution two of the above-mentioned parameters should be as small as possible, i.e., the exposure time, which for moving platforms is directly related to the pixelsize in flight direction, and the field of view, which is directly related to the pixelsize in the direction perpendicular to the flight direction. So for collecting sufficient energy, the spectral bandwidth and the brightness of the system should be as large as possible.

The spectral band for panchromatic sensors is in general chosen from 500 to 700 nanometre corresponding to that of the human eye. The blue region (400 to

500 nm) is not included because these region is often disturbed by atmospheric influences. Sometimes the spectral band is extended up to 800 nm. This gives the advantage that a lot of energy reflected by vegetation is included and also that the vegetation can clearly be recognised in the images. Within the panchromatic images differences between objects with different colours but the same intensities cannot be observed.

Examples of panchromatic sensors are SPOT-PAN, IRS, KVR-1000, Orpheus, and almost all planned high spatial resolution optical satellites.

#### Multispectral recordings

Multispectral sensors contain a limited number of spectral bands (3 to 10). The spectral bands are defined by spectral filters which only pass light within a certain spectral region, generally with a bandwidth of 10 to 30 nanometre. By choosing three spectral bands in the blue, green and red a colour image corresponding to the human eye is obtained, but many other combinations are possible.

Because of the smaller spectral bands the spatial resolution (and/or the radiometric resolution) of the multispectral images is in general less than for panchromatic images. The spectral bandwidth is in the order of 10 to 100 nanometre, also depending on the spatial resolution which has to be obtained, and on the spectral information to be gathered.

Most multispectral sensors have at least three bands: green (550 nm), red (550 nm) and near infrared (850 nm). These three bands are represented as a false colour image, in blue, green and red respectively. Within these images most information which is sensed by the human eye is represented plus information from the vegetation, which is represented in the near infrared channel. A lot of sensor systems do only have these three bands, like SPOT, IRS and photocameras. Some multispectral sensors do have more spectral bands:

- Blue band (400 nm). Combined with the green and red band this gives natural colour images. Also this band contains information on the atmosphere so that it can be used for the atmospheric correction of the other spectral bands.
- Bands in the near and middle infrared (900 to 2500 nm). These spectral bands contain information on the vegetation (chlorophyll up to 1000 nm and water content in the plant leaves 1500 nm) and soil moisture.
- Thermal infrared bands. For information on the soil temperature and human activity.

Examples of multispectral sensors (with within brackets the number of bands) are Landsat-MSS (4), Landsat-TM (7), SPOT-XS (3), CAESAR (9).

#### **S1.1.2 Imaging geometry and image distortions**

The images as acquired with remote sensors can be influenced by several distortions, both geometrically and radiometrically.

##### Geometrical distortions:

- Sensor system. As a consequence of the sensor principle the image can be geometrically distorted. For example in case of a rotating mirror there will be an S-band distortion. Also as a consequence of sensor inaccuracies distortions

will occur, for example because of a not ideal lens or mirror. In general these distortions are corrected before delivery of the images to the user.

- Platform movements. As a consequence of variations in platform movements or platform rotations, image distortions can occur. For satellites the distortions in general are limited, but for aircraft the distortions can be very severe. In case the movements are sensed and recorded, corrections for the distortions can be made afterwards.
- Sensor imaging geometry. In case of a wide field of view there will be a lot of variation in the viewing direction and as a consequence in the image geometry. Also when a sensor is pointed sideward or forward geometric deviations exist.
- Curvature of the Earth. As a consequence of the curvature the image is distorted. Also due to relief, objects and features are displaced. Thirdly, the Earth's rotation causes geometric distortions.
- These distortions in principle can be corrected in case the source of distortion is known with enough accuracy.

#### Radiometric distortions:

- Sensor. As a consequence of inaccuracies in the sensor system radiometric distortions may occur, like striping as a consequence of different characteristics of the individual sensor elements, or temporal variation of the sensitivity. Also variation over the acquired image may occur as a consequence of the difference in viewing direction over the image.
- Atmosphere. Especially in satellite images, but clearly also in airborne images atmospheric degeneration of the image radiometry will occur as a consequence of reflection and transmission effects. If enough information on the atmosphere is present corrections can be made.

### **S1.1.3 Present and future systems**

#### **Spaceborne systems**

Because satellites are operating at larger altitudes the spatial resolution of spaceborne systems is in general worse. Especially for civil remote sensing satellites the spatial resolution during the past two decades was not better than 10 meter.

However at this moment major developments are taking place. Many countries are involved in a development programme for remote sensing satellites. Coming years more than ten different optical satellite systems will be launched, of which most have spatial resolutions of less than 10 meter.

A second development is the better relation between the Eastern and Western countries in the world. During the last years both in the United States and in Russia old spy-satellite images with resolutions of some meters are sold commercially.

Related to this is the decision of the United States to allow a number of commercial companies to acquire satellite imagery with spatial resolutions of up to

1 meter. After this decision at least three companies started the development of 1-meter resolution satellites for commercial use.

As a consequence of these developments the availability of satellite imagery will improve significantly. In the past due to the limited number of satellites the observing rate (frequency of coverage) of areas on earth was rather low, especially for military applications. With the large number of satellites for the coming years the frequency will increase considerably.

An overview of the present and future civil and military earth observation satellites is given in the Table below.

System	Country	Launch	pan		XS			stereo	revisit
			resol. m, <sup>1</sup>	scene km	resol. m	bands nr <sup>2</sup>	scene <sup>3</sup> km		
<b>Civil</b>									
Landsat-1-5	USA	1972->	-	-	30	7BMT	185	-	16
Landsat-7	USA	1998	15	185	30	7BMT	185	-	16
SPOT-1-3	France	1986->	10	60	20	3	60	ac	5-7
SPOT-4	France	1997	10	60	20	4M	60	ac	5-7
SPOT-5	France	1999	5	60	10	4M	60	al/ac	5-7
KVR-1000	Russia	1996	2(an)	40	-	-	-	ac	-
KFA-1000	Russia	1977->	5-8	80	-	-	-	ac	-
MK4	Russia	1977->	-	-	8-12	3	144	ac	-
JERS-1	japan	1992	-	-	24	8BM	75	al	44
IRS-1C	India	1996	6	70	23	4M	141	ac	5
ADEOS	Japan	1996	8	80	16	4B	80	ac	5
ALOS	Japan	2000	2.5	70	10	4B	7-	al/ac	5-7
EarlyBird	USA	1996	3	3	15	3	15	ac/al	3-5
QuickBird	USA	1997	1	27	4	4B	27	ac/al	1
OrbView	USA	1997	1,2	8	4	4B	8	ac	2-3
Space Imaging	USA	1997	1	13	4	4B	13	ac	1-3
CTA-Clark	USA	1996	3	?	15	3	?	al	?
TRW-Lewis	USA	1996	5	?	30	384BM	-	?	
CBERS	China/Brazil	1996	20	113	20	4B	113	ac	5-7
KOMSAT	Korea	1998	10	?	10	?	?	?	?
<b>Military</b>									
Helios 1A&B	France	1996	1	?	?	?	?	?	3-5
Helios 2	France	2000	0.5	?	?	?	?	?	3-5
Ofek-3	Israel	1996	1-2	?	-	-	-	?	?
KeyHole-12/3	USA	1996	0.1	?	?	?	?	y	3-5?

<sup>1</sup> The resolution for analogue images (photographs), indicated with '(an)', is given after scanning.

<sup>2</sup> All multispectral sensors have green, red and near-infrared; possible extra bands are blue (B), extra near-infrared (N) or mid-infrared (M).

<sup>3</sup> Stereo imaging can be across track (ac) or along track (al).

### Landsat TM

Landsat is a satellite operated by NASA for scientific objectives, but more and more also for commercial use. Up to now 5 versions have been launched starting in 1972. At this moment Landsat-IV and Landsat-V are operational. Landsat-VI was lost during launch in 1995 unfortunately. Landsat-VII is planned for launch in 1998.

All Landsat satellites were equipped with the MSS Multi-Spectral Scanner, a relatively low resolution (80 meter) sensor. Besides this Landsat-I to III were equipped with a videocamera RBV (red/visual/blue), which was replaced by the Thematic Mapper (TM) for the newer satellites (II and IV).

The Thematic Mapper sensor is an optical electro-mechanical scanner, which means that the image is built up pixel by pixel and line by line with a single detector element for every spectral channel.

The Thematic Mapper has 7 spectral channels:

band	spectral window	spatial resolution
	(micrometer)	(meter)
1	0.42 - 0.52	30
2	0.52 - 0.60	30
3	0.63 - 0.69	30
4	0.76 - 0.90	30
5	1.55 - 1.75	30
6	10.4 - 12.6	120
7	2.09 - 2.38	30

As can be seen the Thematic Mapper has spectral channels in the visible region, including the blue, in the near-infrared, in the middle-infrared, and in the thermal-infrared. This makes the sensor very valuable from a spectral point of view. A disadvantage is the relative low spatial resolution. For most military purposes this is far too coarse. However, for evaluation of land use and distinction between different types of forest, or temperature variations over larger areas, the sensor can still be of use.

The Landsat satellite has a circular, sun synchronous, near polar orbit. The first three Landsat satellites had an orbit altitude of 919 kilometres, the later satellites 705 kilometres. For the Landsat-IV and V this means that the satellite can image an arbitrary area on the world every 16 days.

A scene of the Thematic Mapper covers an area of approximately 185\*185 kilometre. For the test areas of Heerde and Freiburg quarter scenes were used.

### SPOT

The French SPOT satellite is a commercial satellite of which starting from 1986 up to now 4 satellites have been launched. Presently SPOT-2 and -3 are active.

The SPOT satellites are equipped with two sensors, a panchromatic sensor (PAN) with a spatial resolution of 10 meter, and a multispectral sensor (XS) with a spatial resolution of 20 meter. The sensors are long arrays of CCD-elements which image the terrain line by line (pushbroom type).

The multispectral sensor has only three spectral bands:

band	spectral window	spatial resolution
	(micrometer)	(meter)
1	0.50 - 0.59	20
2	0.61 - 0.68	20
3	0.79 - 0.89	20
pan	0.51 - 0.89	10

Compared to Landsat SPOT has a higher spatial resolution. From a spectral point of view the sensor has less spectral channels, 3 instead of 7 by Landsat. As a consequence of the pushbroom sensor type the geometry and radiometry of the SPOT sensors is better than that of the Landsat sensors.

An important feature of the SPOT satellites is the ability to point the sensors sideways across the track from -27 to +27 degrees. As a consequence of this the satellite is more flexible to acquire images of a specific area. The reaction time for imaging an area can be shortened to 3 to 5 days.

A second consequence of the pointing capability is the ability to acquire stereo-images, two images of the same area acquired from a different point of view. With these stereo pairs Digital Elevation Models (DEM) can be generated with accuracies of about 7 meter standard deviation.

A SPOT scene covers about 60 by 60 kilometer.

### KVR-1000

The KVR-1000 camera is part of the Russian military earth observation programme KOSMOS. Starting from 1962 Russia has launched a large number of short-duration photographic reconnaissance satellites. These are satellites of the Kosmos- or Resurs-type. The satellites have a relatively small mission duration of 2 to 4 weeks, and a relatively low orbit which slowly changes from about 450 to 170 kilometres.

One of the cameras mounted on the satellites is the KVR-1000, an analogue photcamera with a 1000 millimetre lens. The camera takes panchromatic images at an average altitude of 220 kilometre with a resolution of about 2 meters. The scene size is about 80\*80 kilometre.

The quality of the KVR-1000 images is rather bad. During the scanning procedure of the analogue photographs dust on the negatives is also scanned. The radiometry of the photographs is not so good and is worsened further by the scanning procedure, resulting in saturated and black parts in the image.

The images out of the image archive are scanned and sold by the WORLDMAP organisation. In general the ordering procedures take more time than those for other satellite data.

Both for Heerde and Freiburg KVR-1000 images were used.

**Airborne systems**

Airborne sensor systems are relatively flexible compared to spaceborne systems. A wide range of platforms is available operating from altitudes of 100 m up to 25 km, capable of carrying payloads of several kg to several tons, operating from one hour up to several days.

During flight operator interaction is possible. Instrument modifications can be applied and tested very flexible.

As a consequence of these features a wide range of airborne sensor systems is available.

**Civil airborne sensor systems:**

In the following Table an overview is given of several civilian available airborne sensors of the mentioned types:

Sensor	spec. nr.		ch.		mir	tir	radiom. quality	bits	FOV deg	min.alt 100 m/s	min.res. at 1 km	pixels	size cm	stereo capab	other
	vis	nir	nir	vis											
A1:															
Analogue camera															
Leica Wild RC20	3	y	y	-	-	-	anal.	56-120	-	0.15-0.3	-	-	±170kg	y	
Zeiss RMK Top	3	y	y	-	-	-	anal.	56-120	-	0.15-0.3	-	-	±170kg	y	
A2:															
Digital camera															
Kodak DCS 420	3	y	-	-	-	?	12	16	?	0.3	1012*1524	10*10	y	35mm cam	
Kodak DCS 420 CIR	3	y	y	-	-	?	12	16	?	0.3	1012*1524	10*10	y	35mm cam	
THOR	1	-	-	-	y	0.1 K	?	20	?	?	256*197	?	y		
B1:															
Multisp. scanner															
CAESAR (push)	9	y	y	-	-	500	12	24	2000	0.5	1728	40*50*30	y	experim.	
Daedalus:															
ATM (whisk)	12	y	y	y	y	?	12	86	800	1.0/2.0	720	?	-	commercial	
TIMS (whisk)	6	-	-	-	y	?	8	86	1600	4.0	720	?	-		
B2:															
Imaging spectr., pushbr.															
CASI	15	y	y	-	-	200	12	34	758	0.9	512*288	?	-		
WIS-2	84	y	y	-	-	?	12	19	758	0.5	512*512	?	-		
AISA	16	y	y	-	-	?	12	21	667	0.7	384*288	12*17*22	-	commercial	
TRWIS III	384	y	y	y	-	400	12	13.1	877	1.7/2.9	256	44*65*52	-		
Imaging spectr., whiskbr.:															
DAIS2815	28	y	y	y	y	?	15	82	2000	2.0/5/10	512-2048	?	-		
DAIS7915	79	y	y	y	y	?	15	78	2000	2.2/6.6/10	512-2048	?	-		
Daedalus:															
AHS	48	y	y	y	y	?	12	86	1600	4.0	720	?	-	commercial	
Wildfire	50	-	-	y	y	?	?	?	?	?	?	?	-		
MIVIS (AA5000)	102	y	y	y	y	100	12	71	2000	4.0	754	70*50*70	-		
C:															
Video-cameras:															
Silvacam	3	y	y	-	-	45	8	38*25	?	?	670*492	?	y		
IR18	1	-	-	-	y	0.38 K	8	38*25	?	?	370*250	?	y		

### Military airborne sensor systems:

In general military airborne optical sensor systems do have other characteristics than civil systems because of:

- The larger operating speed of the military aircraft, in the order of 200 meter/second;
- The wide range of operating altitudes of the military aircraft; vfrom ery low altitudes of 100 meter to very high altitudes of about 25 kilometres;
- The required very high spatial resolution for reconnaissance (decimetre level).
- The limited number of spectral channels required; panchromatic or maximal three spectral channels.

Up to now analogue photographic framing cameras, like the camera in the Dutch Orpheus pod operated by SQ306, are used because of their high spatial resolution. An often used camera is the KS-87 camera of Recon Optical Instruments. Lenses with a focal length of up to 300 mm are used. These cameras are also used within the Dutch Mars-pod.

During the last years more and more digital systems are under development, because of the advantages in the handling of the digital data. The acquired digital images can be transmitted to the ground using a datalink. No film development process is required. The data can be integrated easily with other available data (historical image data, scanned maps, GIS vector and administrative data). Report generation and distribution of the information can be done easily.

The radiometric quality of the digital data in general is better. The spatial resolution often is somewhat worse.

Examples of digital sensor systems are digital line scanners, like the ATARS-sensors. Both a Low-Altitude and a Medium-Altitude Sensor sensor is available with scan frequencies of up to 2500 Hz and linear CCD-arrays with 12000 elements. As described above already the geometric stability of the linescanners is not so good.

Relatively new are the digital framing cameras. At this moment cameras with CCD-arrays with 5000\*5000 elements are available. An example is the Recon Optical CA-260/25 camera which can acquire 2.5 frames of 5000\*5000 pixels per second.

Because of the central projection also stereo information can be obtained. A new development is the step-frame-operation which directs the camera in steps accross the flight direction so that a wide field of view is generated.

Especially in the UAV's, which have a smaller flying speed and of which some operate at low altitudes, video-cameras are used with large variable zoomlenses of which the data can be easily transmitted to a ground receiving station. Examples are the Sony 999 QTY2 camera and the infra-red Mitsubishi IR-5120 CIV camera used in the Predator.

### CAESAR

CAESAR (CCD-Array Experimental Scanner for Applications in Remote sensing) is an airborne multispectral scanner, developed by NLR and TNO-TPD. The CAESAR system consists of 4 cameras which each have three linear CCD-arrays in the focal plane.

By placing spectral filters for the detector arrays spectral channels can be defined. Different sensor modes with maximal 9 spectral channels in parallel can be defined.

The scanner has a relatively high spatial resolution, depending on the flight altitude and speed, and on the scanning frequency. Resolutions up to 0.4 meter can be reached. By recording accurate flight parameters the images can be corrected geometrically after the flight with an accuracy of 2 to 3 pixels.

The scanner also has a high radiometric resolution as a consequence of the radiometric correction which is applied for every single detector-element.

Because of the different viewing directions of the three CCD-arrays in every camera, and also because of the ability of one camera to be pointed forward, stereo images can be acquired.

With CAESAR images of the Heerde test area have been acquired. The system has been flown at an altitude of 6 kilometres with the Landmode filterset. This filterset consists of three bands:

band	spectral window	spatial resolution
	(micrometer)	(meter)
1	0.54 - 0.57	1.5
2	0.66 - 0.69	1.5
3	0.85 - 0.90	1.5

The resolution of the images is 0.75 \* 1.5 meter. The swath width is 2600 meter. In total 5 tracks of 20 kilometre length have been flown from west to east so that a total area of 10\*20 kilometre was covered.

All data have been radiometrically and geometrically corrected to a grid with a pixelsize of 3\*3 meter, and afterwards a mosaic has been made.

A small part of the data set, the western half of track-2, was processed with a higher resolution of 1.5\*1.5 meter.

### AVIRIS

AVIRIS (Airborne Visible and InfraRed Imaging Spectrometer) is an imaging spectrometer flown on the NASA ER-2 aircraft. From an altitude of 20 km a 10 km swath is covered. The resolution is 20 m.

The data contains 224 spectral bands ranging from 380 nm to 2500 nm. The average bandwidth is about 10 nm.

## S1.2 Thermal infrared sensors and image data

### S1.2.1 Physical background

#### General

A fundamental difference with optical and microwave remote sensing is that the images obtained in the thermal infrared wavelength region are more characterized by environmental conditions rather than by the properties of the objects in the images. There are two thermal infrared wavelength regions (8-12 micron and 3-5 micron). The first region is appropriate to measure surrounding temperatures (typically 0 - 20 degrees Celsius). The second region is appropriate for measuring heat sources like running engines, exhausting pipes, chimneys etc., which can have temperatures of 100 degrees Celsius or more.

All objects emit electromagnetic radiation (i.e. thermal radiation) as a function of their temperature and a factor called the emissivity. The sensor measures this radiation and in this way images can be obtained showing so-called radiant or apparent temperatures as pixel values. The radiant temperature is related to the physical temperature by:

$$T_{\text{rad}} = \epsilon \cdot T_{\text{phys}}$$

where  $\epsilon$  is the emissivity, which indicates how well an object can radiate. Shining objects can for example radiate less easy than dark objects.

From the above it is clear that an image only shows contrast between the objects when their temperatures differ and/or when their emissivity differs. In the thermal infrared region emissivities do not vary drastically so that the main driving parameter for contrast in the image is the physical temperature.

Differences in temperatures occur especially when objects are heated (for example by the sun) or are cooling. Temperature differences occur therefore especially in the morning or evening. The rate of heating or cooling is determined mainly by the heat capacity of an object. For natural objects the water content is important in this context, since the heat capacity of water is rather high.

The atmosphere is also quite important for two reasons:

- 1) atmospheric water content influences the transmissivity of the thermal infrared radiation. Since the sensor is located on a flying platform with often a long line of sight, this is important. High atmospheric water content diminishes the transmission of the radiation resulting in less contrast in the image. This effect is quite severe at 8-12 micron and can even prevent monitoring. This problem is less severe at 3-5 micron.
- 2) the atmosphere can indirectly heat and also cool the environment.

Other factors important in thermal infrared images are:

- 1) heat sources, like engines, fires and heating in houses and other buildings show up in the images.

- 2) healthy vegetation regulates its temperature by regulating the evaporation of moisture. The evaporation needs energy and reduces therefore the temperature, preventing the vegetation from becoming too warm on a warm sunny day in the summer. Vegetation will therefore often show less contrast in thermal infrared images.

Earth surface features emit radiation energy primarily in the thermal infrared region with wavelengths in the range of 3 - 12  $\mu\text{m}$ . This radiation can be detected in order to obtain information about objects. This type of detection is called thermal infrared remote sensing. The amount of radiation energy that is emitted by an object is characterized by the heat flux, which is the heat transfer rate in a direction per unit area perpendicular to the direction of transfer.

Most thermal remote sensing is performed in the 8 - 12  $\mu\text{m}$  region of the electromagnetic spectrum because here the atmospheric effects are small. Such a region is called an atmospheric window. Another atmospheric window is located between 3 and 5  $\mu\text{m}$ . Applications of thermal remote sensing are evaporation, rock type and structure determination, and volcanic studies.

In the following we will give some more details about temperature, emissivity and sensor properties.

### Temperature

All natural objects emit radiation energy as a function of their temperature and the frequency of the radiation. Just as the total energy emitted by an object varies with temperature, the frequency at which the maximum emission occurs also varies with temperature. This phenomenon is illustrated by a piece of iron which is being heated. As the object becomes progressively hotter, it begins to glow and its color changes successively to higher wavelengths, from red to orange, to yellow and eventually to white.

### Emissivity

A quantity describing the emission of energy by an object is its emissivity. The emissivity is the ratio of energy emitted by an object and the energy emitted by a hypothetical ideal object, at the same frequency and with the same temperature for both objects. The hypothetical object is called a blackbody and it has the properties that it totally absorbs and re-emits all incident radiation energy. Natural objects only approach this ideal. For instance the sun is a good example of a black body. A blackbody has an emissivity of 1. An important property of the emissivity of an object is that the emissivity always equals the absorptivity, which basically means that the absorbed radiation is always equal to the emitted radiation.

Most natural bodies have a constant emissivity in the 8 - 12  $\mu\text{m}$  region of the electromagnetic spectrum. These bodies are called greybodies and this region can be used to assess the *radiant* temperature of the object.

The radiant temperature of an object corresponds with the thermal energy which is emitted by the object. It is calculated from the heat flux by means of Planck's equation. Radiant temperature is also known as the apparent temperature.

Emissivity (or absorption) is directly related to reflectance: the higher an object's reflectance, the lower its emissivity. For instance water has a negligible reflectance and an emissivity of almost 1. This is in contrast with a sheet of metal which has a high reflectance and an emissivity much less than 1. A low emissivity leads to an interesting phenomenon: a large metal structure can be warm or even warmer than its surrounding background, but its radiant temperature is lower due to its low emissivity. These properties also result in significant diurnal effects. For instance a lake with water appears cooler than its surroundings at daytime and warmer at nighttime, because water stores heat very well. This storage property is known as thermal capacity (heat capacity) since it is analogous to the electrical capacity.

### S1.2.2 Imaging geometry and image distortions

#### IFOV

A thermal image is obtained by rotating a mirror which is placed in front of a thermal detector, which can be mounted on an aircraft for instance. The rotation is along scan lines which are perpendicular to the flight direction. In this way a thermal image is obtained from a swath under the aircraft.

With a thermal detector radiation is sensed within the instantaneous field of view (IFOV). The IFOV of a thermal detector is defined as the cone angle  $\Delta\theta$  (see Figure S2) in which the radiation is focused on the detector. The IFOV defines the spatial resolution of the system. Just like for optical sensors (see section S1.1.2) the diameter of the sensed ground segment varies because the distance between the detector and the segment varies. Like in section S1 the dimension of the resolution cell ( $\Delta\rho$ ) varies with

$$\Delta\rho = H * \text{IFOV} / \cos(\theta) = \Delta\rho_0 / \cos^2(\theta)$$

where  $H$  is the height of the sensor,  $\theta$  is the angle between nadir and the line of sight and  $\Delta\rho_0$  the resolution at nadir. This distortion results in image scale compression, which increases from nadir. Note that the distortion only occurs in the along scan direction, so perpendicular to the flight direction. Because of this distortion the interpretation of an image becomes difficult near the edges. The image can be rectified by determining the ground positions of the image points, but resolution loss near the edges is inevitable.

### **S1.2.3 Present and future systems**

#### **Spaceborne systems**

##### Landsat Thematic Mapper

The Landsat satellites (originally called Earth Resources Technology Satellites) began in 1967. Landsat 4 and 5, launched respectively in 1982 and 1984, both carried the Thematic Mapper sensor which operates in the thermal infrared region of the electromagnetic spectrum. Band 6 is a thermal infrared band between 8 and 12 micron. The resolution is however only 120 meter compared to 30 meter for the other bands.

##### NOAA/AVHRR

Several generations of satellites have been flown in the NOAA (National Oceanic and Atmospheric Administration) series. The NOAA-6 through NOAA-10 missions, in the period 1979 - 1986) contained the AVHRR (Advanced Very High Resolution Radiometer), which measures in the thermal infrared region of the electromagnetic spectrum. The resolution is 1 km.

##### METEOSAT

METEOSAT was especially designed for the observation of cloud properties and dynamics from space. It operates in three bands, with one thermal infrared band. The resolution is 5 km.

#### **Airborne systems**

##### TIMS

TIMS (Thermal Infrared Multispectral Scanner) is a multispectral scanner that operates exclusively in the thermal infrared region of the spectrum. It is deployed from a NASA Learjet C-130 flying at 22 km, the swath width is 12 km and the resolution is 25 m.

## S1.3 Microwave sensors and image data

### S1.3.1 Physical background

#### The SAR concept

The SAR (Synthetic Aperture Radar) concept is based on the fact that in the flight (azimuth) direction of an air- or spaceborne radar, every image element of the illuminated area is being observed during some time interval. The movement of the radar during this time interval will result in a Doppler frequency shift in the signals returning from the image elements. The Doppler frequency shift depends on the relative velocity of the radar with respect to an image element.

In order to comprehend the SAR concept, the cross section of the antenna beam in the flight direction is illustrated in Figure S3. The beamwidth of the antenna perpendicular to the the flight direction is  $\beta$ . The radar is at slant range (i.e the length of the line of sight)  $d$ . So the radar illuminates an area with a size  $\beta \cdot d$ . A certain image element of this area, denoted as  $x$ , is being observed for the first time when the radar is at position 1. This image element is some portion of the ground surface, which is fixed in space. Since the radar is moving there will be a moment that the image element is not observed anymore. This is the moment when the radar is at position 2, and the radar has then moved in the flight direction over a distance  $\beta \cdot d$ .

The SAR concept uses the fact that the movement of the radar between positions 1 and 2 can also be viewed as if there is only one radar, but with a very large antenna. When now the radar signals reflected at  $x$ , and obtained at positions between 1 and 2, are recorded together with their phase history, a synthetic aperture can be constructed by applying specific summing operations on those recorded signals. Theoretically this synthetic aperture can have a length of  $\beta \cdot d$  and with antenna theory it can be found that the corresponding beamwidth then becomes  $\lambda/(2\beta d)$ , where  $\lambda$  is the wavelength of the electromagnetic radiation. It so appears that this SAR illuminates an area with a size  $(\lambda/2\beta d) \cdot d = \lambda/2\beta$  in the flight direction. From antenna theory it follows also that  $\beta = \lambda/l$ , with  $l$  the length of the antenna. Therefore, the resolution of this SAR becomes  $l/2$  and is independent of the distance between the radar and the illuminated area. In practice, however, the resolution will be worse, which will be explained later.

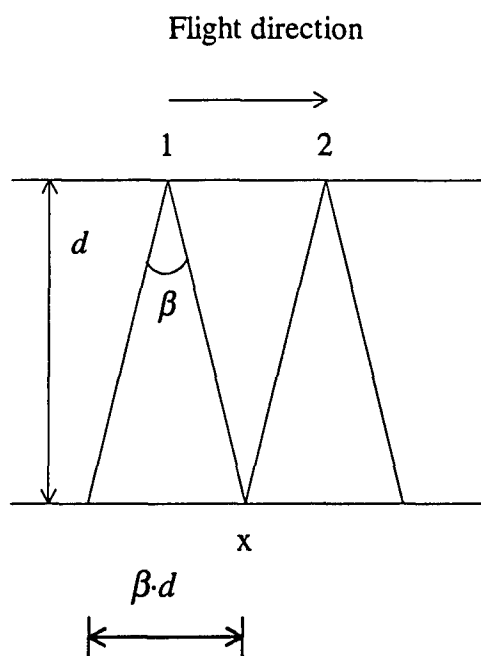


Figure S3: Explanation of the SAR concept.

### Backscattering types

Microwave remote sensing data is gathered by measuring the strength of the energy that is scattered by an object in response to energy transmitted. A measure for the amount of scattering is the scattering coefficient for the surface material being illuminated. This coefficient is a function of the electrical permittivity of the material, and the roughness and shape of the object in comparison to the wavelength of the microwaves. To obtain insight in the coefficient it is worthwhile to consider the types of scattering that can occur in nature.

Smooth surfaces (depicted in Figure S4a) act as specular reflectors. Almost all incident radiation is scattered away from the transmitting radar. As a consequence such surfaces appear dark in a radar image. This scattering type is called *specular scattering*. On the other hand when the surface is rough then the incident energy is scattered in all directions and part of this energy is scattered back towards the radar (see Figure S4b). This second type of scattering is called *rough surface scattering*.

Scattering due to vertical structures like buildings, fences, trunks etc. usually occurs by so-called *double-bounce* or *corner* reflections (see Fig. S4c). One reflection is due to the ground surface and one to the vertical wall. These reflections are quite strong, but are extremely sensitive to their orientation towards the radar: the reflection is only seen in the image when the wall is oriented exactly parallel to the flight path, i.e., perpendicular to the line of sight of the radar. SAR images of a build-up area therefore consist of a greyish image with bright spots and lines on places where streets and buildings are parallel with the flight path.

For scattering from vegetation this situation is somewhat different. If there is an object on the surface e.g. a tree (see Figures S4d and S4e) then a different type of scattering occurs. The microwaves will interact with the tree canopy, and it will generally be very difficult to define where exactly in the canopy this interaction takes place. A part of the microwaves will be scattered back to the radar directly (Figure S4d) and a part will be scattered to the radar after a reflection by the soil surface (Figure S4e). The first type of scattering is called *volume scattering*, whereas the second type is called *surface-volume interaction*. These types will lead to a light tonal appearance in a radar image.

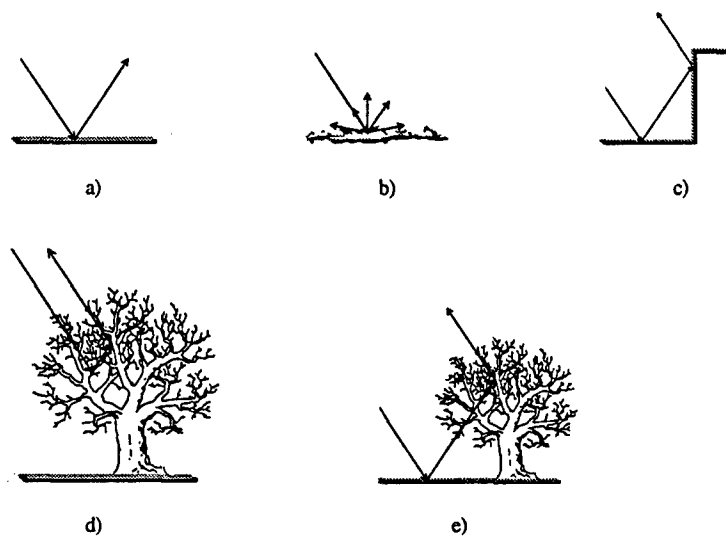


Figure S4: The Figure depicts the different types of backscatter as encountered in radar image data: a) specular, b) rough surface, c) corner reflector, d) volume, and e) volume-surface scattering.

### Resolution and speckle

A radar transmits energy during some time interval. This interval is called the pulse length  $\tau$  of the radar. In order to distinguish two elements, which are located somewhere in space at a mutual distance  $L$  in the same direction relative to the radar, the reflected signals from these elements must necessarily be received at different times. The time difference between reception of the two reflected signals must be at least  $\tau$ , the duration of the transmitted pulse, because otherwise the two elements will be seen as one element. The time difference between reception depends on the distance  $L$  between the two elements, because the microwaves propagate with the velocity of light ( $c$ ). If now the reflected signals from the two elements have travelled over some distance, say  $R_1$  and  $R_2$ , then it follows that  $R_2 - R_1 = 2L$ . So in order to distinguish the two elements it must be that  $c \cdot \tau \leq 2L$ . The minimum distance between the two elements then becomes  $c \cdot \tau / 2$ . This minimum distance is called the range resolution of the radar and is illustrated in Figure S5. Recall that the resolution in azimuth is given by  $\beta \cdot d$ . A radar resolution cell has, therefore, an area with dimensions  $c \cdot \tau / 2$  in range and  $\beta \cdot d$  in azimuth. However, in

a practical situation this resolution area is not obtained because of specific operations which reduce an unwanted effect.

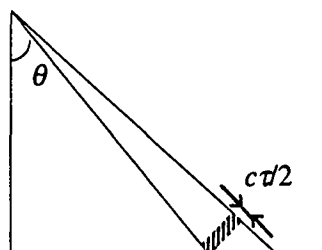


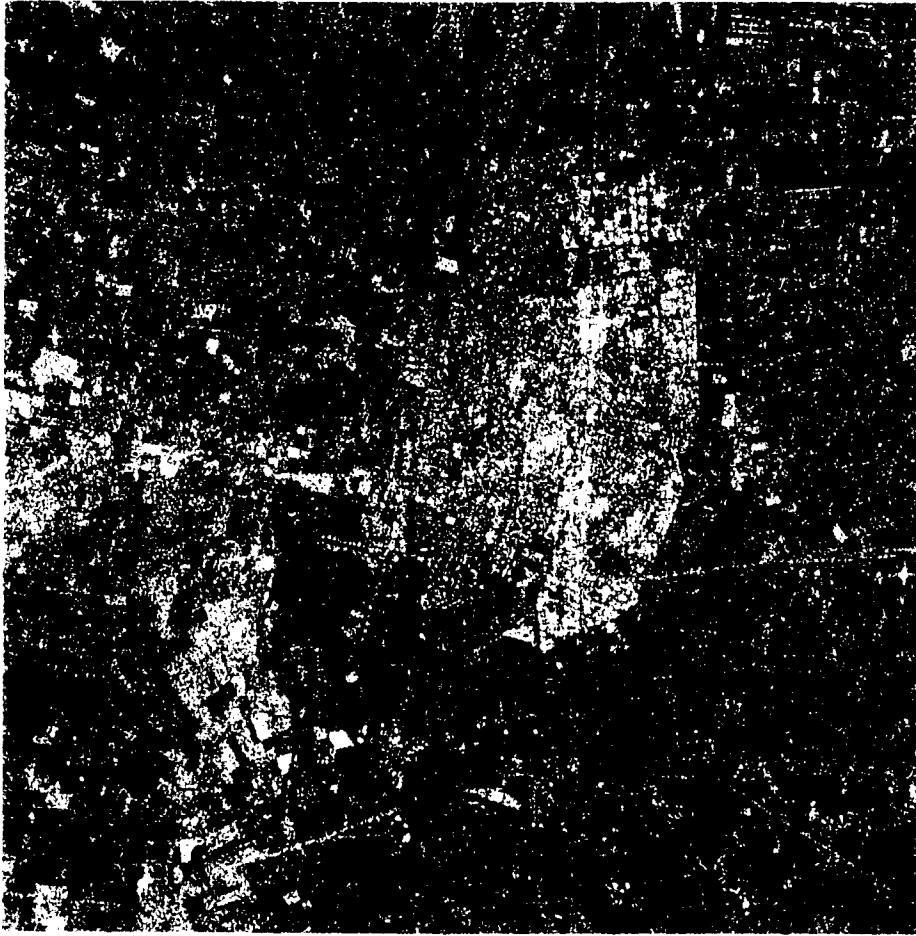
Figure S5: The range resolution of a radar.

A detailed analysis of a radar image shows that important variations occur between adjacent resolution cells. This effect, caused by the coherent electromagnetic waves used by the radar systems, is called speckle. Speckle is the statistical fluctuation or uncertainty associated with the intensity of each pixel in an image.

The physical mechanism that produces the speckle in an radar image is interference. Many natural objects such as the tree in a previous example, consist of a number of scatterers that can move because of wind. As a result the reflected signals in a resolution cell originate from continuously changing scatterers, and the phases of these signals change accordingly. In a measurement the received signals from these scatterers are added and therefore, the total intensity fluctuates. A single look SAR image archives one estimate of the reflectivity of each resolution cell in the image. Speckle may be reduced at the expense of resolution, in the SAR processing by averaging several looks. Such an image is called a multi-look image. A multi-look image can also be obtained by averaging images of exactly the same area, but recorded at different dates.

We show here an example (Figure S6) for the ERS satellite of the city Leeuwarden and its air base. The multi-look image is obtained by averaging 8 images recorded over a period of 2 months.

## Multi-temporal multi-looking



## ERS image



## Speckle reduced ERS image

Figure S6: Speckle suppression by multi-temporal multi-looking.

Speckle noise influences the ability to discriminate between different objects, e.g. field boundaries, roads etc. It is therefore necessary to account for the number of looks, a measure for the speckle, when spatial resolutions of microwave and optical images are compared. We define therefore the effective spatial resolution for microwave images by:

$$\rho_{eff} = \rho(1 + 1/\sqrt{L})$$

where  $\rho$  is the resolution and  $L$  the number of looks. For the ERS and JERS this means that with a resolution of 25 meter and a number of looks of 3, the effective resolution which can be compared with resolutions in the optical and thermal infrared is about 40 meter. For PHARS the resolution is 6 m and the number of looks is 7 so that the effective resolution is about 8.5 m.

### Polarisation and polarimetry

An electromagnetic wave consists of a magnetic and an electric field vector. The polarisation of an electromagnetic wave is defined by the direction of its electric field vector in a reference plane perpendicular to the direction of propagation. A radar generally transmits a plane, monochromatic wave, which basically means that the electric field vector is rotating in the reference plane and the tip of this vector describes an ellipse. Figure S7 illustrates the reference plane with the so-called polarisation ellipse.

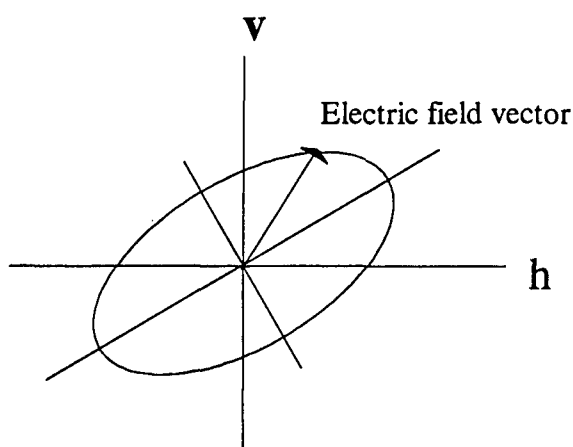


Figure S7: The polarisation ellipse.

In Figure S7 the v- and h-directions denote vertical and horizontal. Electromagnetic waves with their electric field vector in the v- and h-direction are called vertically and horizontally polarised respectively. The direction of propagation of the wave is into the paper.

Conventional radars measure the amplitude of the scattering coefficient by transmitting and receiving microwaves with a single polarisation. This polarisation

depends on the antennas used for transmit and receive. A polarimetric radar transmits and receives both horizontally and vertically polarised waves. In this way more information about the illuminated object is obtained than with conventional radars. This technique is called polarimetry.

### **Phase and interferometry**

The phase of an electromagnetic wave gives information about the state of a wave, that is, whether a crest or a trough occurs in the wave at a given moment and place. The occurrence of crests and troughs in a wave can result in the interference phenomenon. When two waves (with the same wave length) are in phase the crests in the waves will add and a wave results with an intensity which equals the sum of the intensities of the two interfering waves. When the two waves are out of phase the crests and troughs will add and a wave results with an intensity which equals the difference between the intensities of the two interfering waves. So it can be that the two interfering waves extinguish, when they have equal intensities.

Radar interferometry is based on two images of the same area, but with a slight difference between the positions of the radar. The phase information of the two images is then superimposed. The two phase values at each pixel are subtracted, which leads to a so-called interferogram. These phase differences give the altitude variations of each pixel and so enable the generation of a Digital Elevation Model (DEM).

### **S1.3.2 Imaging geometry and geometrical distortions**

Radar imagery is based on the fact that the position of an object is determined from the time interval between the moment that energy is being transmitted and the moment that reflected energy is received. As a consequence in a radar image the position of an object relative to the radar is found. The distance between the radar and object is called slant range and the so obtained image is called a slant range image. This image is subject to two types of distortion:

1. scale distortion;
2. relief distortion.

#### **Scale distortion**

This type of distortion concerns the difference between a slant range and ground range image. With the aid of the angle between the radar look direction and the vertical (the incidence angle), and the altitude of the radar it is possible to convert a slant range image into a ground range image. This conversion is less complicated for airborne systems than for spaceborne systems since in this latter case also the curvature of the Earth plays a role.

#### **Relief and height distortion**

Since relief influences the distance between the surface and the sensor, distortions occur in the range geometries. Also the local incidence angle is influenced by the relief. This can give three types of distortions in:

1. Resolution loss
2. Radiometric darkening and brightening
3. Displacement

These distortions are generally present in images of mountainous areas. In general 4 effects due to relief are discriminated which contain one or more of the above mentioned distortions. The are three main types: *foreshortening*, *layover* and *shadowing* and a less important effect which is called here *darkening*. These effects are exemplified in Figure S8. Foreshortening and darkening can in principle be corrected when a digital elevation model (DEM) is available, while layover and shadowing are anomalies where information is lost.

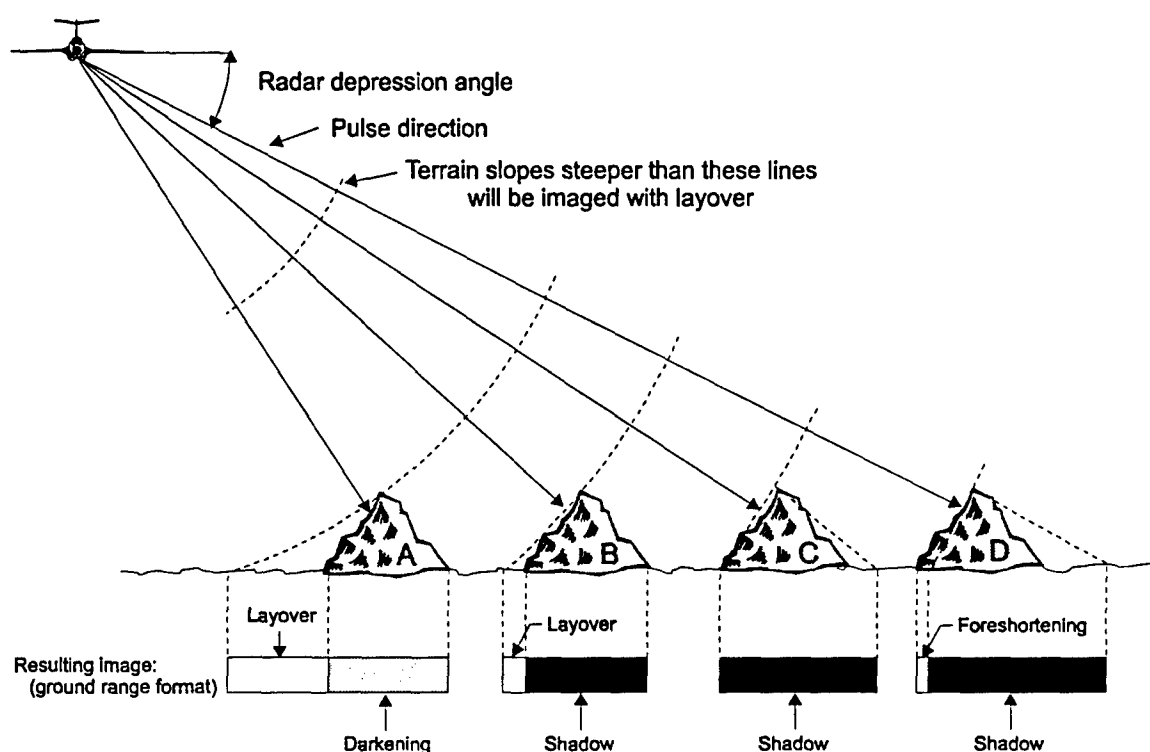


Figure S8: Effects of relief on a radar images.

Taking as example a mountain ridge parallel to the flight path foreshortening and layover occur on the front side of the mountain while darkening and shadowing occur on the backside. Which effect occurs depends on the slope angle and the look angle of the sensor. In Fig. S9 we show a plot of the look angle versus the slope angle. In this plot the four areas where these effects occur are indicated. Layover occurs when the slope is so steep that the top is illuminated before the foot of the mountain, so that the top of the mountain is projected before the foot of the mountain. This occurs for smaller look angles and larger slope angles. Images of mountainous areas from the ERS satellite having a small look angle of 20 degrees therefore often suffer from layover. When the slope angles are smaller and/or the look angles are larger foreshortening occurs. Areas with foreshortening suffer from resolution loss and to a lesser extent from displacement and brightening (radiometric distortion) The latter two distortions can be corrected with a DEM.

On the back side often mountain shadowing occurs when both the look angle and the slope angle are larger, since the mountain blocks the line of sight between the radar and the dale behind the mountain. For smaller look angles and slope angles darkening occurs. Areas with darkening suffer mainly from radiometric distortion and from displacement. Since darkening can be completely corrected using a DEM, it is a less serious effect than foreshortening where always non-correctable resolution loss occurs.

Summarising for small scale and moderate scale relief only foreshortening and darkening occurs while the choice of look angle is less crucial. For large scale relief lay over or shadowing occurs depending on the choice of the look angle. It is not possible anymore to avoid one of these anomalies. A solution is to image the mountainous area from two opposite sites and to make an optimal choice for the look angle (see Fig. S9).

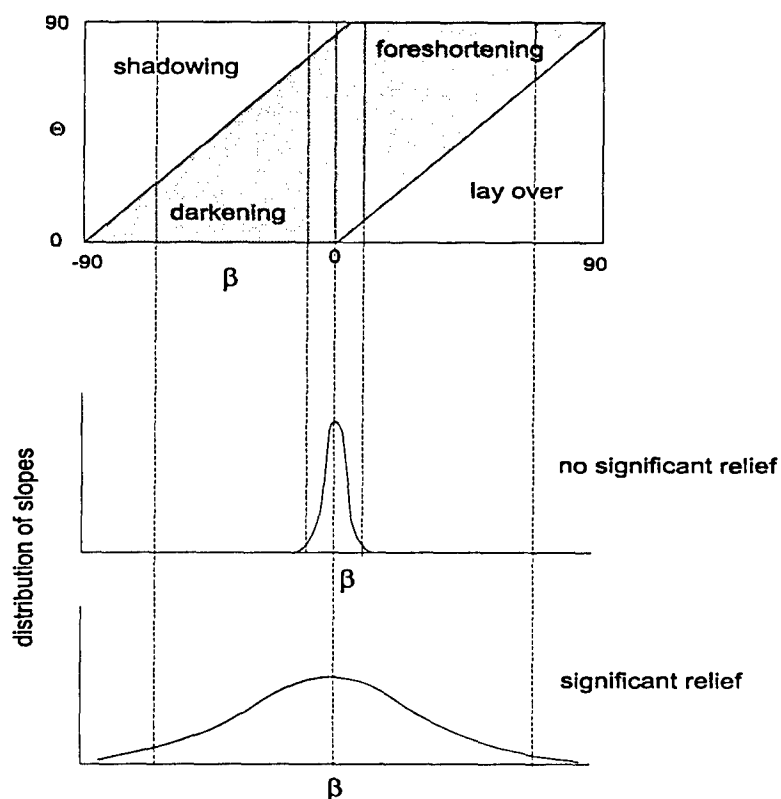
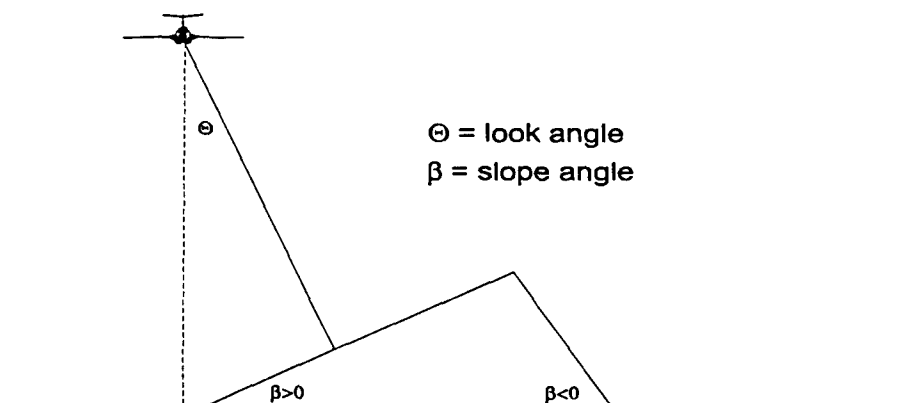


Figure S9: Relation between look and slope angles and relief distortion.

A related effect is that reflections from the top of high buildings, high tension pylons etc precede reflections from the ground so that they appear to be shifted towards near-range. The same is true for forest edges. In these cases also so-called double bounce reflections often occur where the reflection is both due to reflection from the ground and the building or forest. In the image these bounce reflections are located near the foot of the buildings and forest edges. On the other side of the building or forest shadowing is seen for the same reason as mentioned in case of relief.

### S1.3.3 Present and future systems

#### Spaceborne systems

##### ERS-1

The ERS-1 satellite was launched on 17 July 1991 by ESA. It is an earth-observation satellite mainly designed for oceanographic applications, but it has also provided useful data for land applications. Among other instruments the ERS-1 carries a SAR with a resolution of about 30 m (four looks) and operates at a frequency of 5.3 GHz and VV-polarisation. The incidence angle is fixed at  $23^{\circ}$ . In April 1995 ERS-2 was launched, which carries a SAR with basically the same specifications as the one onboard the ERS-1. Because these identical SAR systems are both operational, a special configuration has been defined, the so-called tandem mode. This mode was used from August 1995 until May 1996 and enabled the collection of interferometric SAR image pairs, which can be used for Digital Terrain model sets.

##### JERS-1

The Japanese Space Agency NASDA has launched the JERS-1 satellite on 11-2-92. This satellite carries a L-band SAR (1.3 GHz), which operates at a fixed incidence angle of  $35^{\circ}$  and HH-polarisation. The resolution is 18 m (three looks).

##### RADARSAT

In November 1995 the Canadian RADARSAT satellite was launched. It carries a SAR operating in the C-band with variable incidence angles ( $20^{\circ}$  to  $45^{\circ}$ ), HH polarisation, and a resolution of about 30 m (four looks).

##### ENVISAT

The ENVISAT platform is scheduled for launch in 1998 and will carry a SAR operating in the C-band, with HH and VV-polarisation's, a resolution of 30 m, and a variable incidence angle in the range  $23^{\circ}$  -  $45^{\circ}$ .

##### EOS-SAR

The EOS-SAR (Earth Observation System- Synthetic Aperture Radar) will be operating at L-, C- and X-band. It is intended that the SAR operates at incidence angles in the range  $15^{\circ}$  -  $52^{\circ}$ , with a variable resolution between 30 and 500 m. Measurements are to be made with both co- and cross-polarisations (HH, VV, HV and VH for the L-band, and HH and VV for the C- and X-band). It is planned to launch this SAR in the late 90's.

##### LACROSSE

US military spaceborne SAR. This sensor can be operated in spotlight mode delivering images with resolutions in the order of 1m.

## Airborne systems

### PHARS

The PHased ARray Synthetic aperture radar is a testbed for its polarimetric successor PHARUS. This Dutch sensor is build and operated by TNO-FEL, NLR and the technical university of Delft. The radar uses the C-band and VV polarisation. Its nominal resolution is 6 m with 7 effective looks. Typical swath width is 6 km with incidence angles varying between 30 and 70 degrees. Its special feature is the phased array antenna, which enables steering of the beam and makes that the radar is rather compact.

### PHARUS

The PHased ARray Universal Synthetic aperture radar resembles its predecessor PHARS, except that it is polarimetric. Like the PHARS it uses the C-band and delivers images with resolutions down to 3 meter, 5 looks. There are several modes of operation resulting in swath widths ranging from 3 km to 15 km with incidence angles varying from 20 to 80 degrees.

## S2. Visualisation techniques

We discuss here several visualisation techniques. One-layer images like Spot-Pan are visualised as grey tone images. When more layers are available colours are used. For example three layer images like CAESAR images are visualised by showing the layers in the red, green and blue channel (see section S2.1 and S2.2). For multi-layer images with more than three layers (e.g. LandSat) more advanced techniques have to be used to obtain a meaningful visualisation (section S2.3 and S2.4).

### S2.1 False colour and simulated natural colour

Optical sensor systems, used on board of spaceborne or airborne platforms record the data in several spectral wavelength intervals; a number of spectral bands in the visible part of the electromagnetic spectrum and a number of bands in the near infrared.

In a considerable number of occasions sensor systems do not record the blue channel in the visible part of the spectrum, while the green and red part are recorded, as well as one or more infrared bands. Examples of such satellites and airborne platforms are SPOT and CAESAR.

In order to visualise the recorded data one usually takes a selection of three spectral bands: the near-infrared, the red and the green band, and presents those bands in the red, green and blue colour channels, respectively. The image (on screen or film) that is generated in this way is called false colour, meaning that the colours presented are not the real colours as would be observed by the human eye. Generally, in a false colour image, the vegetation appears in several variations of the colour red, the water becomes black or dark-blue and build-up areas appear light-blue to white. For the interpretation of a false colour image one has to have foreknowledge about the way the image is generated in order to interpret the various features in the image correctly.

For several applications one does not necessarily need the false colour information but rather requests for a representation of the true colours, as would also be observed by the human eye.

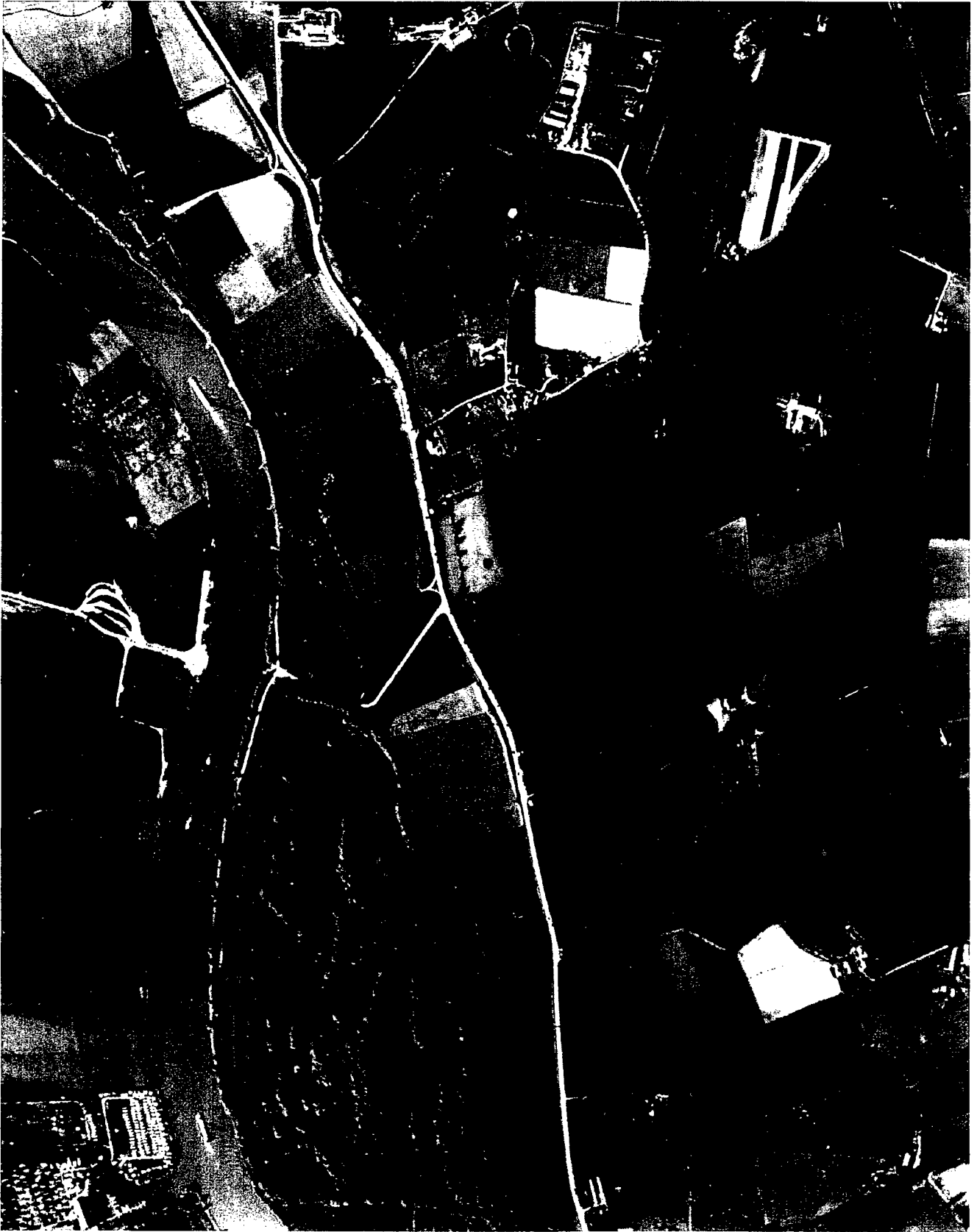
For this purpose an algorithm was developed that uses the recorded information (spectral bands infrared, red and green) in order to calculate an additional blue band. In this way, by selecting red, green and blue, a natural colour combination can be generated. Because the blue band is calculated (not recorded) the colour combination is called simulated natural colour.

From the CAESAR image (acq. date 22-9-94), which is originally in false colour, the simulated natural colour image was derived following the above described method. Both the false colour combination and the simulated natural colour combination are presented in Figures S10a and S10b.



**Caesar false colour image acquisition date : 22-9-94**

*Figure S10a: False colour image of CAESAR with the near-infrared, red and green band shown in the red, green and blue colour channel respectively.*



**Caesar simulated natural colour image acquisition date : 22-9-94**

*Figure S10b: Simulated natural colour representation for CAESAR.*

## S2.2 Combination of panchromatic and multi-spectral images

Panchromatic images are optical images with a relatively high spatial resolution due to the wide spectral band. On these images a lot of detail can be observed. However the images contain no spectral information, which may hinder the interpretation. Multispectral images contain spectral information and can be represented in colour, which facilitates the interpretation. The spatial resolution of the multispectral images in general is lower due to the narrow spectral bands. There are several methods for combining high resolution panchromatic and low resolution multispectral images. In the example shown in Figure S11 a relative simple method was used. The green and red channel of the multispectral image cover the same wavelength region as the panchromatic image. These multispectral channels are now corrected with the variation of the panchromatic channel by the formula:  $[(\text{green})/(\text{green}+\text{red})]*\text{panchromatic}$  and  $[(\text{red})/(\text{green}+\text{red})]*\text{panchromatic}$ , respectively.

The near infra-red channel is not changed and has low resolution. Other more accurate methods which can be used, also accounting for the near infra-red channel, are the IHS (intensity, hue, saturation) transformation or the wavelet-transformation.



*Figure S11: Combination of high resolution (1.5m) panchromatic image with lower resolution (3m) multi-spectral image. Panchromatic image (top), multispectral image (middle), combined image (bottom).*

### S2.3 Principal component analysis

In general, principal component analysis is an enhancement technique where a number of image file bands can be rearranged to new major axes in order to create new bands that express more variance in the data.

For the principal component analysis in the Geographic Remote Sensing project a multi-band file was created, consisting of:

1. CAESAR (3 channels), 22-9-94
2. KVR-1000, 19-5-92
3. TIR, 9/10-94
4. PHARS, 27-9-94

This 6-channel file was used for the analysis of principal components. The analysis puts out two additional files; a table file in which the eigenvalues are presented and a matrix file in which the eigenmatrix is presented. Figure S12 shows the created six components separately as black&white images, the table file (eigenwaarden) and the matrix file (eigenmatrix).

# Principal component analysis on a six-channel image

Combined : Caesar (NIR, R, G), KVR, TIR and Phars



Component 1



Component 2



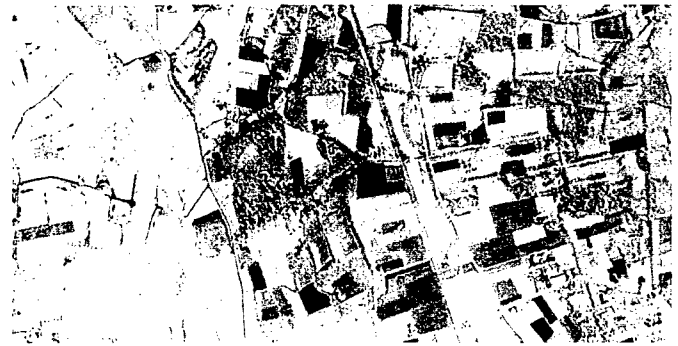
Component 3



Component 4



Component 5



Component 6

## Eigenwaarden

Component	Count	Percentage
1	2372	48
2	1527	30
3	634	13
4	275	6
5	89	2
6	51	1

## Eigenmatrix

Comp. Band	1	2	3	4	5	6
Cae-NIR	0.53	-0.68	0.43	-0.14	-0.06	-0.22
Cae-R	0.30	-0.05	-0.68	0.29	-0.11	-0.59
Cae-G	0.44	-0.18	-0.47	-0.09	0.04	0.74
KVR	0.66	0.69	0.29	0.05	-0.01	-0.03
TIR	0.06	-0.05	0.01	0.19	0.98	-0.07
Phars	-0.02	-0.13	0.21	0.92	-0.17	0.24

Figure S12: Principal component analysis. See text for explanation.

From the eigenwaarden table the contribution for each component to the information content can be deducted. In the eigenmatrix the weight of all six channels per component is expressed, in other words which channels contribute most to a certain component. Analysis of the eigenmatrix leads to the following conclusions:

- **First column (component 1)**  
In this column mainly optical factors; intensity differences between the three CAESAR channels and KVR, these four channels are about evenly strong represented.
- **Second column (component 2)**  
Striking here is the strong negative contribution of CAESAR NIR and the strong positive contribution of KVR. The negative contribution of the CAESAR NIR band can be seen very well in the component 2 image (upper right), these are the shadowed parts in the area (in white). Further, the image shows the changes between NIR and optical **and** the changes in time (CAESAR: 22-9-94 , KVR: 19-5-92). The light parcels in the image are due to CAESAR NIR: no reflectance in NIR, so after inversion from black to white, meaning bare soils.
- **Third column (component 3)**  
This component shows interesting features; a positive contribution of NIR and negative contributions of Red and Green. Through this, differences in vegetation will be enhanced. There are also substantial contributions of KVR and PHARS. In this component, wooded areas are strongly suppressed, the same applies more or less to shaded areas. Certain colour effects from the visible part of the spectrum are strongly emphasised.
- **Fourth column (component 4)**  
This column is of no interest because there is a one-sided contribution of PHARS.
- **Fifth column (component 5)**  
Like column 4, this time due to TIR.
- **Sixth column (component 6)**  
Although the contribution to the total information content is very small (see eigenwaarden-table), this component still contains some interesting features and then especially the colour differences between Red and Green. In the image, red rooftops and reddish soils are very well distinguishable from the rest of the image. If desired, this can be visualised even better through an inverse look-up-table (LUT).

## S2.4 IHS transform and decorrelation stretch

On the six-channel principal component image, two enhancement techniques were applied in order to visualise the information better (see Fig. S13).

1. The components 1, 2 and 3 from the principal component analysis are considered to be the three major axes, expressed in Intensity, Hue and Saturation (IHS). Intensity is the overall brightness in the image and varies from 0 (black) to 1 (white). Hue is the colour of a certain pixel and varies from 0 at the red midpoint through green and blue back to the red midpoint at 360. Saturation is the purity of a colour, varying from 0 to 1. With an IHS to BGR transform, these components are mapped to a new image that shows a lot of information.
2. A decorrelation stretch was applied on the six-channel image. This type of stretch consists, in first instance, of a principal component transformation resulting in more variance between the six channels. Then each component is stretched optimally and transformed back to the original 'data position'. The effect on an image is that in channels that originally were quite correlated, now more variance is created, partly by the introduction of new information (other channels) and partly by the temporary change of the eigenvector. The result is that more colour information is generated in the image.

# Principal component analysis on a six-channel image

Combined : Caesar (NIR, R, G), KVR, TIR and Phars



IHS transform of components 1, 2 and 3 to BGR



Decorrelation stretch of combined (six-channel) image, presented are the three Caesar channels (in false colour)

## **S3. Extraction Techniques**

In this section we discuss extraction techniques. We discriminate here between different classes of extraction.

First of all terrain feature extraction will be highlighted in section S3.1.

Corresponding to the data formats in geographical data bases extraction techniques for features of three spatial dimensions (area, line and point) are discussed in section S3.1. In section S3.2 the vertical dimension of the terrain is studied. We discuss both the large scale and the small scale height determination. In section S3.3 the factor time is introduced and changes are extracted by so-called multi-temporal analysis.

### **S3.1 Terrain feature extraction**

#### **S3.1.1 Area feature extraction and classification**

Area feature extraction or classification is image processing is a method to group or categorise pixel values to a certain number of classes. The classes that are generated correspond to a number of pre-set criteria. In general, there are two ways to classify pixels into a number of classes:

1. supervised (the classification criteria are mainly set by the operator/field expert)
2. unsupervised (the classification is mainly automatically performed by the computer)

#### *Optical supervised classification*

At first the six-channel image (CAESAR, KVR, TIR, PHARS) was taken to perform the classification. Main goal was to distinguish a number of classes, partly based upon spectral characteristics within the image and partly following the feature code attribute list. These considerations led to the following classes to be determined:

1. water (with sediment - flowing waters)
2. water (clear - still waters)
3. agricultural
4. meadow1 (mown)
5. meadow2 (ungrazed, young grasses)
6. meadow3 (grazed)
7. meadow4 (high grasses)
8. meadow5 (river forelands)
9. bare soil1 (light coloured)
10. bare soil2 (medium coloured)
11. bare soil3 (dark coloured)
12. broad-leaved

13. coniferous
14. orchard/plantation
15. isolated buildings
16. continuously build-up
17. infrastructure

Some first test classifications (supervised) were carried out on the six-channel image. Also a test classification was carried out only on the three CAESAR channels. For the above 17 'target classes' training areas were indicated with which the classification was performed. These tests led to following conclusions:

- There is too much difference in acquisition dates to perform a good classification on the six-channel image. It is therefore advisable to take only the three CAESAR channels for classification because those channels contain the most multispectral information. Moreover it is necessary to select an area that falls within one CAESAR track because there is too much radiometric difference between the (mosaic) CAESAR tracks, causing intolerable differences in the classification result.
- The indicating of training areas for target classes 15, 16 and 17 is meaningless; these classes completely disappear in the overlap with several bare soil classes.

Following the conclusions above a new dataset was made, a CEASAR 3-channel image with the following coordinates; ULX=202.000 ULY=483.500 and LRX=205.960 LRY=481.476

Training areas were now indicated for the following target classes:

1. water (with sediment - flowing waters)
2. water (clear - still waters)
3. agricultural (maize)
4. meadow-1 (mown)
5. meadow-2 (ungrazed, young grasses)
6. meadow-3 (grazed)
7. meadow-4 (high grasses)
8. meadow-5 (river forelands)
9. bare soil 1 (light colour)
10. bare soil 2 (middle colour)
11. bare soil 3 (dark colour)
12. bare soil 4 (reddish soils/rooftops)
13. broad-leaved
14. coniferous
15. orchard/plantation

The CAESAR image to be classified is presented in Figure S14. From the CAESAR image, feature space plots were derived, these are two-dimensional diagrams that show the spatial distribution of reflectance values of any two-

channel combination. Consequently, for a 3-channel image, three combinations are possible:

- NIR against Red
- NIR against Green
- Red against Green

The feature space plots from CAESAR channels NIR, R and G are also presented in Figure S14, the upper row in black&white, the lower row overlaid with a rainbow look-up-table.

General analysis of the feature space plots delivers the following information:

- **NIR-Red:** broad distribution of the information, well defined clusters. The two small clusters in the bottom left corner (and along the Red axis) are the water. The large cluster in the bottom right corner represents the vegetation; high reflection in NIR (high values at the NIR axis) and low reflection in the Red channel (low values at the Red axis). The cluster in the middle of the diagram indicates the presence of well defined bare soil classes.
- **NIR-Green:** broad distribution of the information. The vegetation cluster now gets an upward shift because in the Green channel, vegetation also reflects high (similar to the NIR channel). The result is that the clusters are somewhat nearer to each other and therefore less distinguishable compared to the NIR-Red feature space plot.
- **Red-Green:** limited distribution of the information, clusters overlap. This is also illustrated by the fact that the overall cluster is located at the x/y diagonal.

# Classification



CAESAR false colour (NIR-R-G = R-G-B) , acq.date : 22-9-94

## Feature space plots for CAESAR channels NIR, R, G

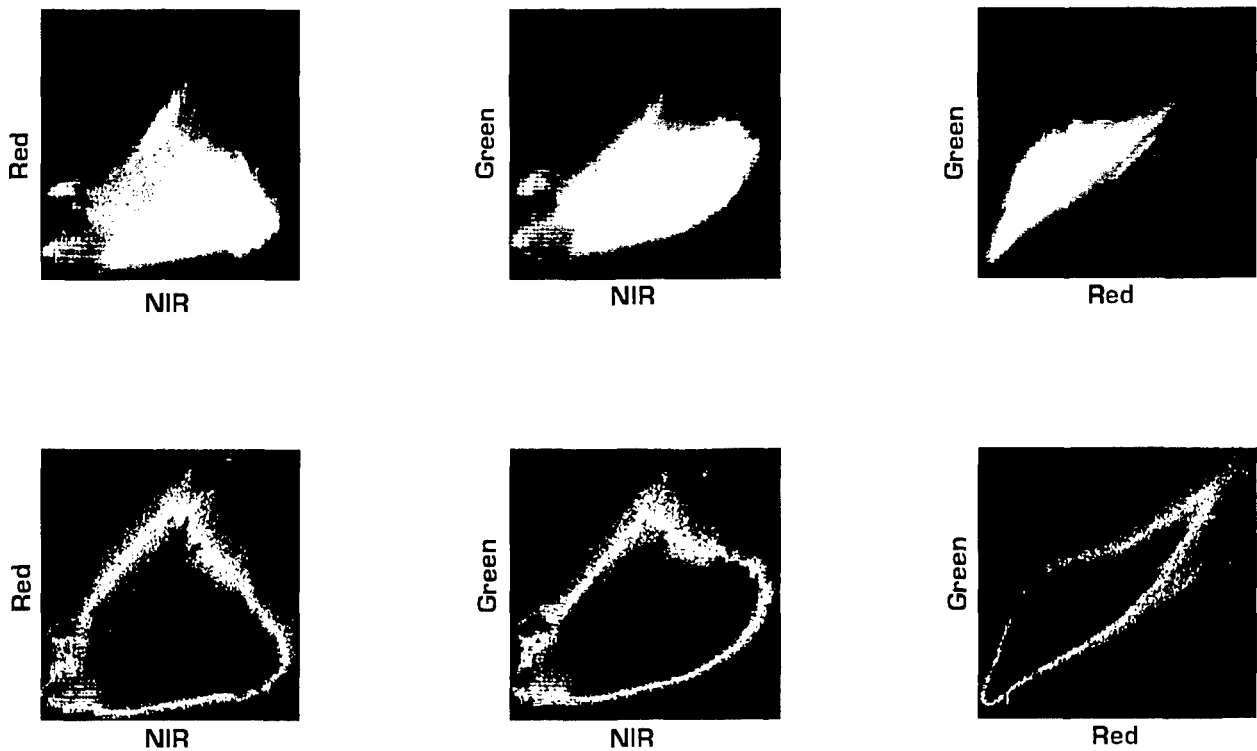


Figure S14: CAESAR image which is used as input for both supervised as well as unsupervised classification. See text for further explanation.

With the already mentioned 15 target classes, a training set was made. The training set is built up by drawing polygons of uniform appearance (for example water) in the image. The pixels contained in the polygon are typically representative for one target class (for example water) and will be used as a reference to assign other similar pixels in the image to that same class. The construction of a training set is entirely based on operator/field expert perception and therefore this classification type is called supervised. After the training set is completed the actual classification can be performed on an image.

# Classification

## Supervised - first round



Classified CAESAR image, acq.date : 22-9-94

### Feature space plots - thematic for CAESAR channels NIR, R, G

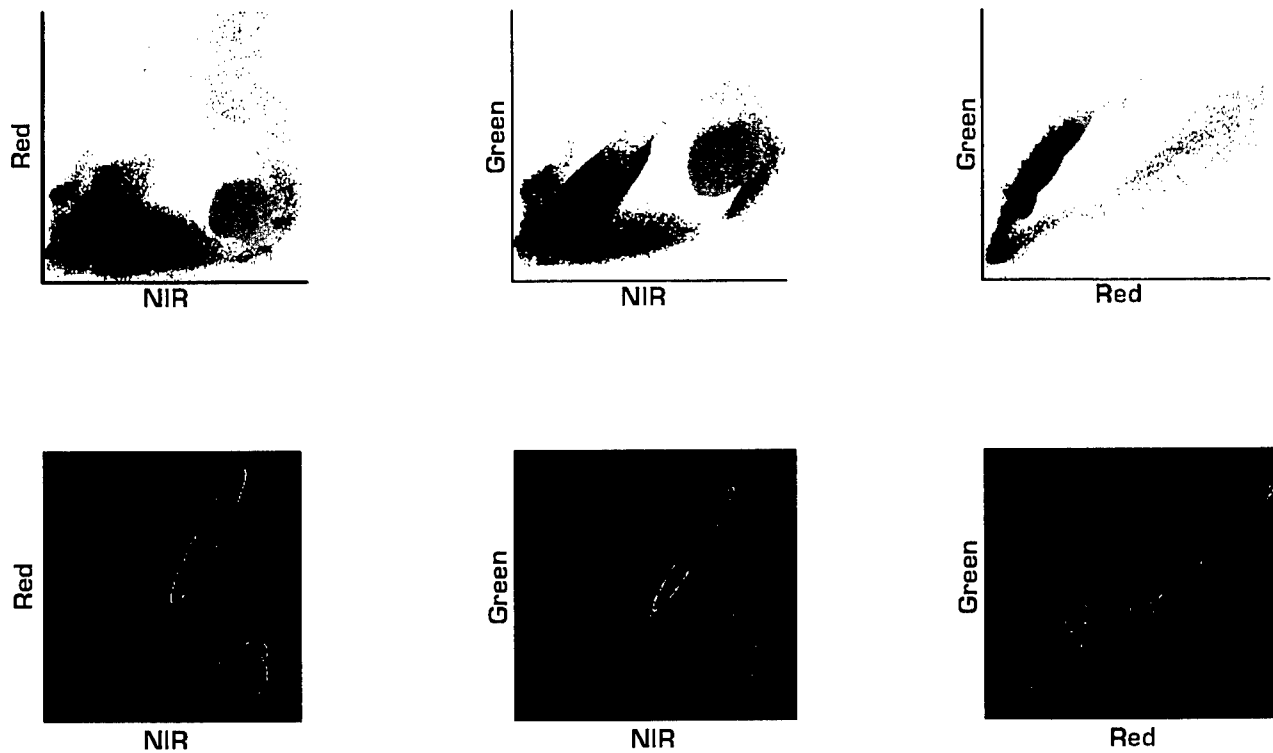


Figure S15: Supervised classification - first round. See text for explanation.

Figure S15 shows the first classification attempt on the CAESAR image with the first training set. Each class in the classified CAESAR image is presented in a uniform colour:

- two blue colours for two water classes
- four grey shades for the four bare soil classes (from dark grey to white)
- ochre for agricultural (maize)
- brown for coniferous forest
- bright green for broad-leaved forest
- five green shades for the five meadow classes
- reddish brown for orchard/plantation

By combining the classified image with the original feature space plots it is also possible to put the classes in so-called thematic feature space plots. These are presented in the upper row in the same organisation as before; respectively NIR-Red, NIR-Green and Red-Green. It has to be noted here that the occurrence of a class in the thematic feature space plot is based on a priority selection of the histogram maxima, in other words the class with the largest number of counts will be assigned to a place in the feature space plot. Because of this one does not see all 15 classes in the feature space plot, for example the colour ochre tells that that class is present at that spot for more than 50% but there can be a substantial presence of other classes which is not visible. Anyway these feature space plots provide very good insight into **where** a class cluster is situated in the feature space, whether they are **homogeneous** or not and the **weight** they bring in. The thematic feature space plots were also presented by drawing the 15 class clusters as ellipses. Now **every** class becomes visible in the feature space plot, as are the class sizes and class overlaps. These feature space plots are presented in lower row in Figure S15.

#### Analysis of Figure S15

In the image both water classes are well classified but the class coniferous forest is also spreading out in between the two water classes. This can especially be seen in the IJssel river area (also in the feature space plot).

The class maize (agricultural) is too broad, it also appears in meadow classes and in dark bare soils.

The class coniferous forest conflicts with a number of other classes like water, meadow and dark bare soil. Coniferous forest also appears in build-up areas, especially in the shadowed parts from the buildings.

The thematic feature space plots show the following:

NIR-Red:

- The two water classes are well distinguishable
- The 4 bare soil classes are lying very near to each other, bare soil 1 has a large spreading.
- Big overlap between broad-leaved and coniferous, the class orchard is entirely included within broad-leaved but is nevertheless strongly marked (small spread).

- The 5 meadow classes as a whole form a very well defined cluster but some of them have large overlap, for example meadow-1 (light green) and meadow-5 (bluish green).
- Maize (ochre) has from itself a large spreading and therefore overlaps with various forest- and meadow classes.

#### NIR-Green:

- Much overlap between maize, meadow classes and forest classes.
- Bare soil 4 (dark grey) is a well distinguished cluster.
- Meadow-1 and meadow-5 overlap much.

#### Red-Green:

- Again a large overlap between meadow-1 and meadow-5
- The class coniferous forest (brown) has too much weight; it overlaps almost entirely with maize and broad-leaved and also spreads out in the direction of water.
- There is overlap between maize (ochre) and sedimented water (cyan).

Following the above analysis a number of actions were taken to adjust the training set in order to perform a second, improved classification:

1. The class coniferous forest will disappear; in this part of the CAESAR image this class is difficult to separate from other classes.
2. Maize will be subdivided into 3 classes (new training polygons have to be drawn).
3. Meadow-1 and meadow-5 will be joined (the new name will be meadow-1).
4. Assign probabilities to all classes (see below).
5. The training set for broad-leaved forest has to be refined.
6. Improve to colour assignment of classes.

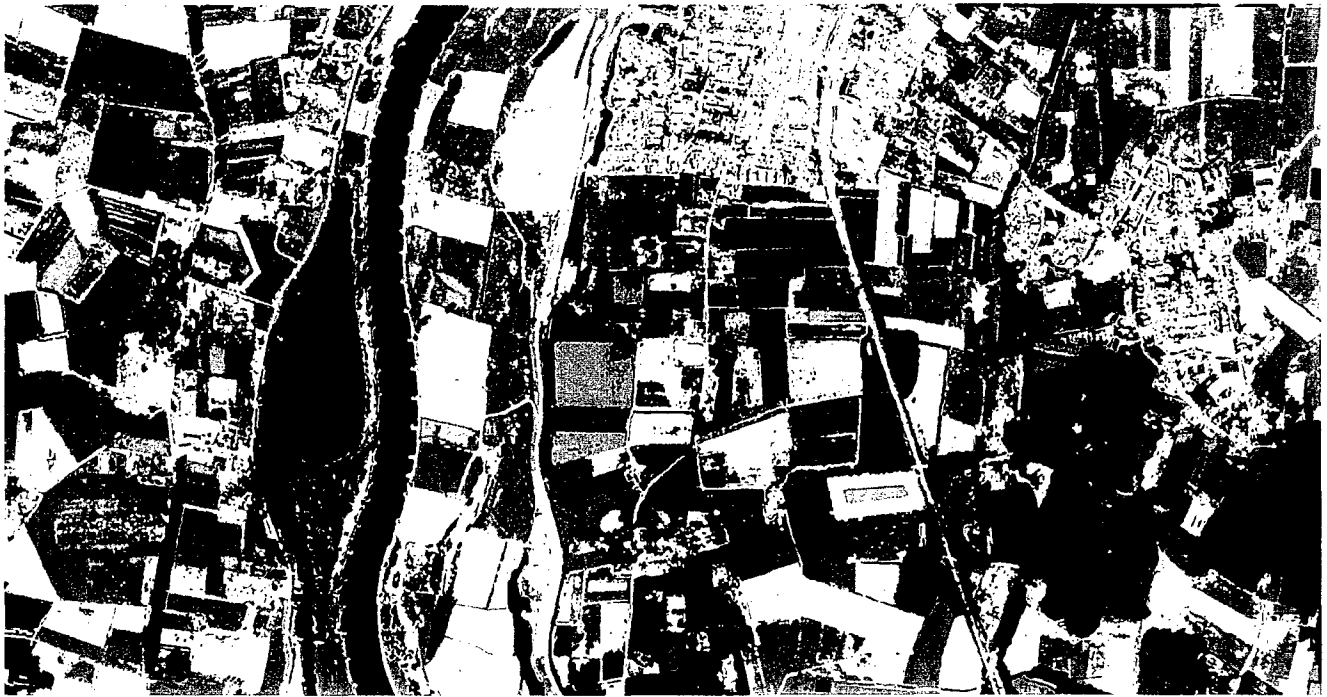
The assignment of probabilities is a way of steering the classification in a certain direction, partly based on pre-knowledge of the information content of the image (the weight of occurrence of certain features) and partly based on experience made with previous classifications. For the second classification of the CAESAR image the following probabilities were assigned:

land	95 %	meadow	70 %	meadow-1	17.5%
				meadow-2	17.5%
				meadow-3	17.5%
				meadow-4	17.5%
		bare soil	7 %	bare soil 1	1%
				bare soil 2	2.5%
				bare soil 3	2.5%
				bare soil 4	1%
		maize	6 %	maize-1	2%
				maize-2	2%
				maize-3	2%
		forest	12 %	broad-leaved	10%
				orchard	2%
water	5 %	water-sediment	2.5%		
		water-clear	2.5%		

After these adjustments the second supervised classification was carried out with the result shown in Figure S16 as well as the accompanying thematic feature space plots.

# Classification

Supervised - second round



Classified CAESAR image, acq.date : 22-9-94

Feature space plots - thematic  
for CAESAR channels NIR, R, G

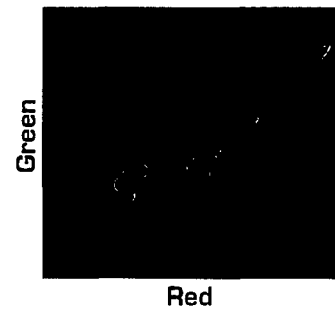
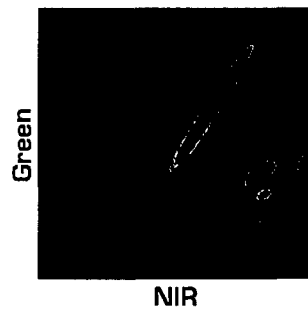
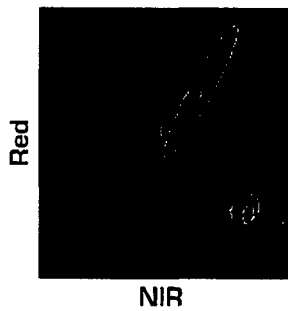
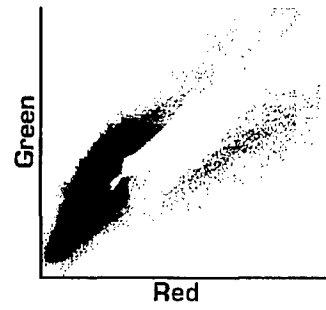
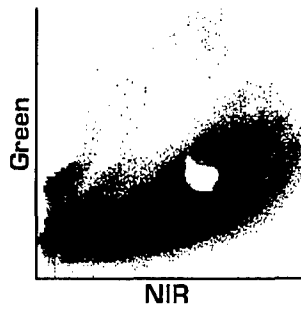
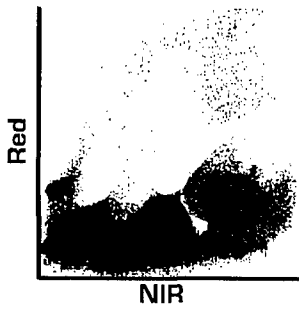


Figure S16: Supervised classification - second round. See text for explanation.

The assigned class colours in the second classification are:

- Dark blue for clear water
- Light blue for sedimented water
- Four greyscale shades for the four bare soil classes
- Three ochre shades for the three maize classes
- Dark green for forest (broad-leaved and coniferous)
- Reddish brown for orchard/plantation
- Four green shades for the four meadow classes

#### Analysis of Figure S16

Compared to the first classification attempt a lot of improvements can be seen in the second classification image. The same applies for comparison of the thematic feature space plots of the first and second classification. Significant features are:

- In general more homogenous classes.
- Correct separation between maize- and meadow classes.
- Improvement in the classification of water, especially for the inland ponds and waterways.
- Better classification of build-up areas and infrastructure.

#### *Optical unsupervised classification*

This classification method is automatically performed by determination of spectral distinctions that are inherent in the data. The method requires minimal input from an operator/field expert, only the number of desired spectral classes has to be given and the number of iterations, these are a number of repeated calculations with increasing refinement because after each iteration new class cluster means are calculated that are used in the next iteration. Most of the operator/field expert work starts after the classification is finished; then the generated spectral classes have to be recognised as thematic classes, and occasionally be grouped or rearranged.

A first unsupervised classification was carried out on the CAESAR image. As input, 15 spectral classes and 6 iterations were given. The classification result is shown in Figure S17. The accompanying thematic feature space plots are also displayed in the Figure. The 15 spectral classes, generated by the classification procedure, have been analysed and then assigned to a certain theme class with associated colour. The following classes were deducted:

# Classification

Unsupervised - first round



Classified CAESAR image, acq.date : 22-9-94

## Feature space plots - thematic for CAESAR channels NIR, R, G

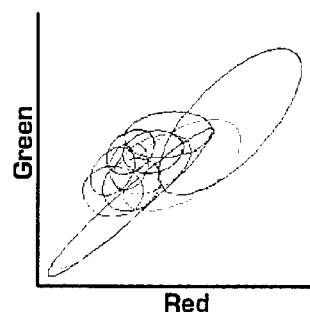
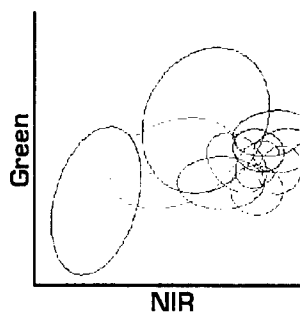
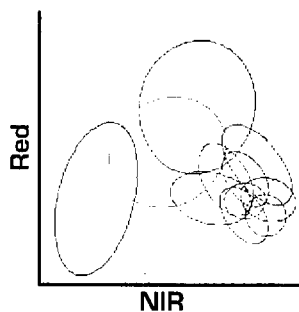
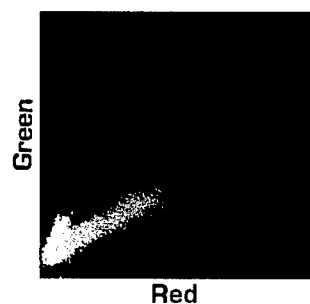
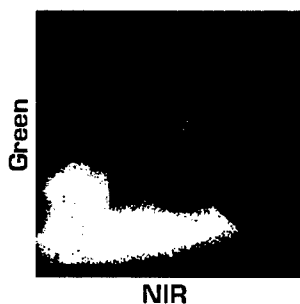
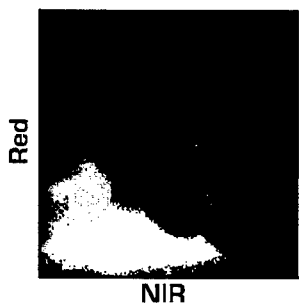


Figure S17: Unsupervised classification - first round. See text for explanation.

water	blue
shadows (dark)	bluish green (dark)
shadows (light)	bluish green (light)
mixed forest	dark green
mixed forest	dark green
bare soil	dark grey
grass/maize	ochre
grass/maize	ochre
grass/maize	ochre
grass	green
bare soil	light grey

#### Analysis of Figure S17.

The classified image shows:

- Water (blue) is also classified in build-up areas.
- The spectral classification procedure puts out two apart classes that represent especially shadowed parts (dark and light bluish green).
- Class 6 and class 15 represent bare soil themes that are apparently spectrally well distinguished (dark and light grey in the image).
- Classes 7 till 14 give all kinds of variations for grasslands and maize. However, grass and maize are not easy to separate from each other.

The colours in the thematic feature space plots do not correspond to the colours in the classified image; they are a discrete presentation of spectral clusters in so-called rainbow colours (from blue through green to red).

In general, the cluster kernels are situated on well distinguished positions in the feature space plots, but due to the spreading of the clusters there is also considerable overlap with adjoining clusters. This can be seen clearly in the lower row of thematic feature space plots (ellipses). For example the water (red ellipse) is quite well isolated from other ellipses but there is also already some overlap with other classes. Overlaps become larger in the 'vegetation corner' in the feature space plots (along the NIR axis). These are all sorts of grass, maize and forest features that are too much mixed in this classification.

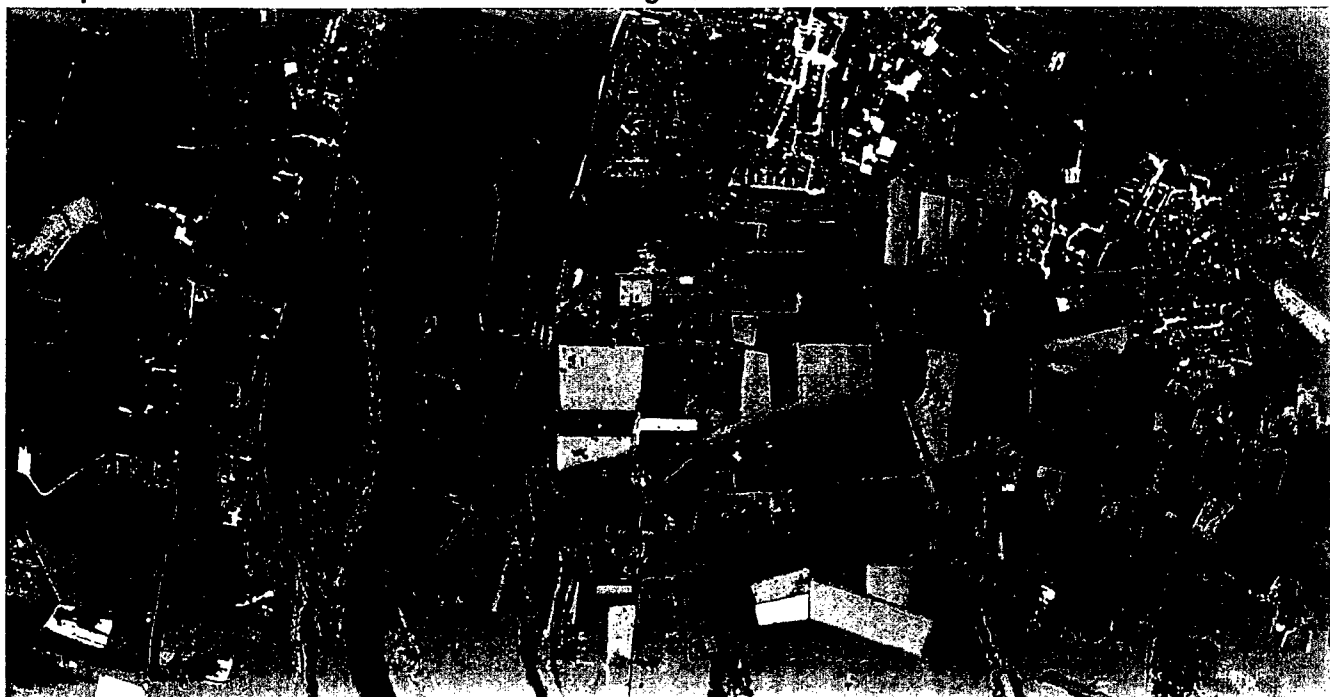
The above analysis of the first unsupervised classification leads to the conclusion that more refinement is needed. Therefore a second unsupervised classification has been performed in which the number of classes has been increased (from 15 to 30) as well as the number of iterations (from 6 to 20).

The result of the second unsupervised classification is presented in Figure S18. This result is not accompanied by thematic feature space plots because firstly the

spatial distribution of clusters is obvious from the first classification attempt and secondly the presentation of 30 rainbow coloured ellipses is not interpretable anymore.

# Classification

Unsupervised classification on CAESAR image (22-9-94)



Legend unsupervised

Class\_Names

	water
	shadow
	mixed forest
	orchard
	grassland
	bare soil
	maize
	bare soil

Legend supervised

Class\_Names

	maize
	grassland
	Water (sediment)
	Water (clear)
	bare soil
	orchard
	bare soil
	mixed forest



Supervised classification on CAESAR image (22-9-94)

Figure S18: Unsupervised classification - second round (top). For comparison also a supervised classification result is shown (bottom). See text for further explanation.

### Analysis of Figure S18

The following remarks are made:

- As a consequence of the doubling of the number of spectral classes to be detected (30 instead of 15), there now is more diversity and specific themes, like maize, can be extracted in a better way.
- Less water in the build-up areas, however there is still a conflict between water and bare soil (see bare soil in the northern part of the IJssel river).
- There is more subtle distinction in all kinds of shadowed areas. Shadowed areas can be extracted quite good so that it is thinkable to use this information for a dedicated image in which heights can be determined.
- Better distinction between maize and grass, maize can now be determined as a uniform class but some conflicts with the grassland classes still remain.
- The orchard class can now be extracted from the (larger) mixed forest cluster, which was not possible in the first unsupervised classification.
- With a spectral classification that generates this large number of classes it also becomes clearer that considerable changes of spectral class signatures exist in the area of interest. For example certain maize classes are determined separately as individual classes east and west of the IJssel river. This implies that for an area of interest that would be bigger than the one that was used now, one should apply segmentation procedures that classify regions as separate entities. Such an extended procedure is obviously time-consuming and was therefore not done in the framework of this study.

As final activity for the classification works on the CAESAR image for the Geographic Remote Sensing study, the second supervised classification and the second unsupervised classification results are compared, which can be observed in Figure S18.

The assigned class colours of both classifications are corresponding to the themes as far this is possible due to the character of the classification method. Specific themes from a certain classification that are not existing in the other classification are presented in a different colour (see the accompanying legends).

A general conclusion with respect to the supervised- and unsupervised classification is that it would be very imaginable to combine the strong points from both classification methods in order to reach a higher accuracy.

### *Microwave classification*

With microwave images it is also possible to obtain (un)supervised land use classifications. Just like in the optical case where it is necessary to have multi-layer (multi-spectral) information in order to perform the classification, multi-layer information is necessary in the microwave case.

Multi-layer imagery can be either multi-frequency imagery, but also polarimetric imagery or an interferometric pair of images.

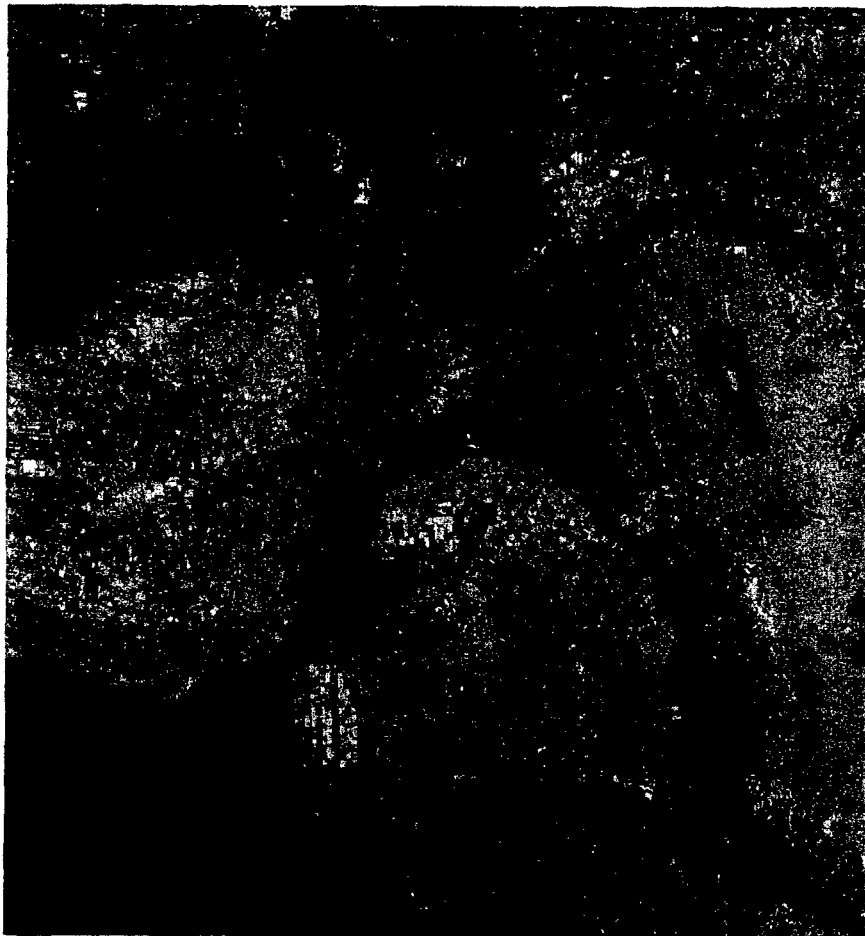
We discuss here for each case an example which can all be considered as unsupervised classification results.

### Multi-frequency land use classification

Multi-frequency microwave imagery is the microwave analogue of optical multi-spectral imagery.

We show here an example (Fig.S19) where we have combined ERS and JERS imagery of the Northern part of the Veluwe and Flevoland, where ERS is displayed in the green and JERS in the red channel. ERS uses a shorter wavelength (C-band, 5.3 cm) than the JERS (L-band, 25 cm). Since the backscattering is different for different land use classes in the C- and L-band classification is possible. For example forest is relatively bright in the L-band, while bare soil is bright in the C-band for example. This happens because physically L-band radiation penetrates vegetation better than the C-band radiation, while C-band radiation is scattered more by rough surfaces than L-band radiation. That is why the agricultural area of Flevoland is green and forests of the Veluwe are orange in the colour composite of Fig. S19. Based on this kind of differences a classification result has been generated that is shown in the right panel of Fig S19.

# Multi-frequency classification



ERS (green) / JERS (red) composite

Class	
■	quiet water
■	windy water
■	low vegetation / grass
■	agricultural fields / bare soil
■	forest
■	urban

Figure S19: Multi-frequency land use classification.

### Polarimetric land use classification

With polarimetric observations the polarisation instead of the frequency is changed. By simultaneously transmitting and receiving vertical and horizontal radiation multi-layer imagery is obtained. These layers are not all equivalent and have different units. Mathematically they can be stored in a matrix:

$$\sigma = \begin{pmatrix} \sigma_{hh} & \sigma_{hhv} & \sigma_{hvv} \\ \sigma_{vh} & \sigma_{vhv} & \sigma_{vv} \\ \sigma_{vhh} & \sigma_{vvh} & \sigma_{vv} \end{pmatrix}$$

where  $hh$ ,  $vv$  and  $hv$  indicate the transmit and receive polarisation combinations. Not all elements of the matrix (i.e. image layers) are in general useful, some of them are usually zero.

Compared to single polarised observations (i.e. only one matrix element is obtained per pixel) now effectively 5 observations are used.

From polarimetric observation more information can be obtained about the scattering process. For example distinction can be made between volume, double bounce and surface scattering (see section S1.3.1). Since these types of scattering are different for different land use classes land use classification is possible.

We show here an example with SIR-C data. These polarimetric C-band data have been obtained during the SIR-C campaign in 1994. The SIR-C radar was located on board of the space-shuttle and the images have resolutions which are comparable to the ERS (25 m, 4 looks).

We show in Figure S20 (top) a colour composite with in the RGB channels the image with the  $hh$ ,  $hv$  and  $vv$  backscatter respectively. Clearly is visible that forests show strong  $hv$  backscatter (green), while soil and build-up areas are purple or pink (strong scattering in  $vv$  and  $hh$ ). Using the full information contained in the matrix (which cannot be shown in a single three colour composite) we obtain the classification result shown in Fig S20 (bottom).



Space borne polarimetric image (SIRC, 5.3 cm) RGB: HH/HV/VV



Polarimetric land use classification

- | class          |   |
|----------------|---|
| water          |  |
| bare soil      |  |
| low vegetation |  |
| forest         |  |
| swamp          |  |
| urban          |  |

Figure S20: Polarimetric land use classification.

### Interferometric land use classification

Two microwave images from the same sensor and of the same area can be averaged to produce a mean backscatter image and subtracted to produce a difference image showing changes. Since microwave images also possess phase information, the phase difference for each pixel in the image can be obtained by correlating the images. The correlation is performed by a 'complex' multiplication of the amplitude images defined by:

$$I_1 \otimes I_2 = A_1 A_2 e^{i(\varphi_1 - \varphi_2)}$$

where  $I_1$  and  $I_2$  are so-called single look complex images containing phase information and where  $A_1$ ,  $A_2$  and  $\varphi_1$  and  $\varphi_2$  represent the amplitude and the phases for each pixel. Essential point here is that the phase difference  $\varphi_1 - \varphi_2$  can contain information. The phase difference can be shown in a phase image or a so-called interferogram, used in section S3.2 to obtain height information. When useful information is available a fringe pattern can be seen (see Fig. S30, bottom right). If no useful information is available noise is present.

Another way of showing the information contained in the phase differences is to produce a coherency image where neighbouring pixels are averaged. The effect is that when no correlation exist (noise in the phase image) the pixel values are zero and when information is available the pixel values are one. Intermediate values are also possible. The coherency image can be considered as a measurement for the information content of the phase difference.

We have therefore three independent images:

1. mean backscatter
2. difference image
3. coherence image

In Figure S21 we show these three image for testsite Freiburg where we have used images from the ERS1/2 tandem mode. These are the same images as used for the large scale height determination in section S4.2.1

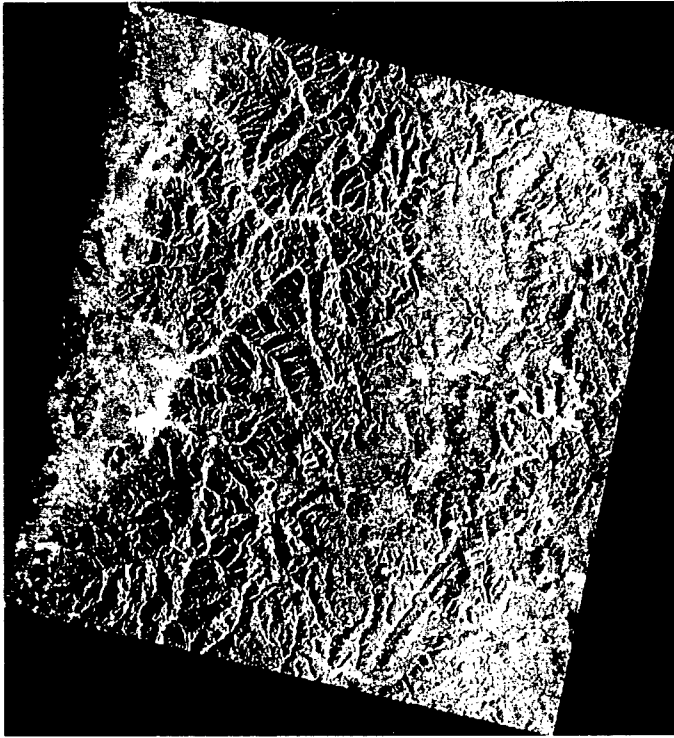
We also combined the images in three RGB colour channels, where the backscatter image is shown in the red channel, the coherence image in the green channel and the difference image in the blue channel.

As we discuss in section S3.2 images of the same area are only correlated when recording takes place from almost exactly the same position in space. Also minor changes of the surfaces can cause decorrelation, which is often the case for vegetation and especially forest. The images in Figure S21 were recorded with an one day interval and it appears that forest areas are decorrelated, while most other areas are not.

In the colour composite therefore forested areas are red, while other areas like agricultural land are green.

Build-up areas are colour yellow/orange since they show high backscatter.

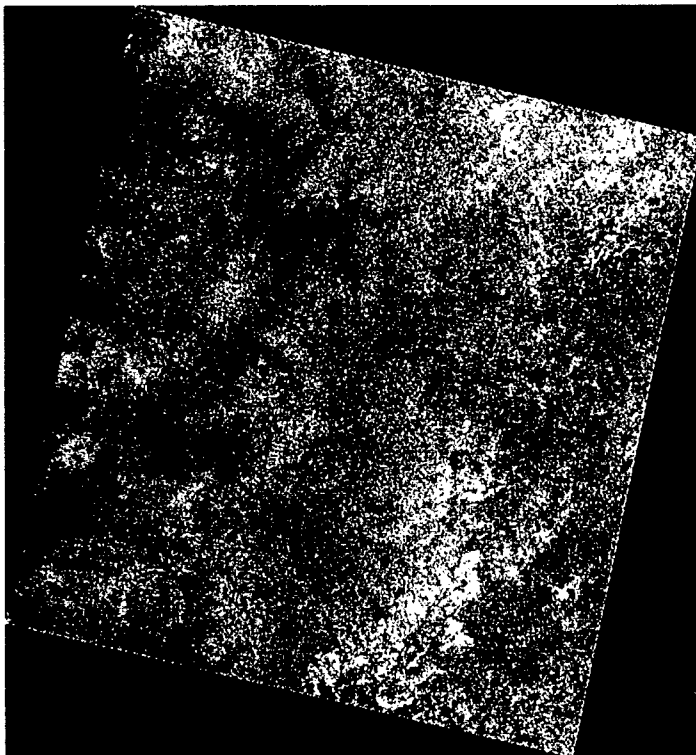
Inspection of this image gives thus land use information. It is not yet a classification results with thematic information, but can be used as input for a classification procedure.



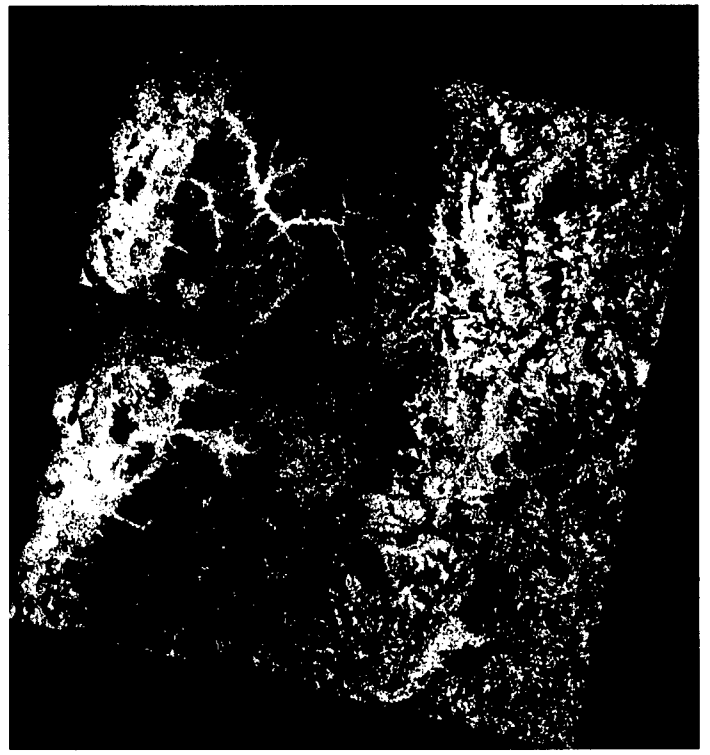
**Backscatter**



**Coherence**



**Difference**



**Land use**

RGB: backscatter, coherence, difference

*Figure 21: Interferometric land use classification.*

### S3.1.2 Line feature extraction

In the previous section we have discussed classification results which are stored as polygons (areas) in a GIS database. In a GIS database line features as well as points can be stored. We discuss here the line feature extraction. We discriminate here between automatic line extraction by a computer and manual line extraction performed by an interpreter. Typical example of line features in images are roads. Roads are usually present in remote sensing images

#### *Automatic line extraction*

The basis for the detection of line features is the difference in radiometric values for the pixels in an image. When a radiometric change is big enough going from a pixel to a neighbouring pixel it can be detected by so-called edge detectors. Lines are then extracted using a threshold (the change should be big enough) and certain decision rules, like the minimum length and the maximum width of a line. A problem in automatic line extraction is that lines are often interrupted mostly due to the abovementioned thresholding. A lower threshold minimises interruption, but also introduces smaller and less relevant lines, so that no optimal solution exist. A typical result is shown in Figure S22 for the Heerde test area. The lines are extracted from a SPOT image. When this result is compared with the roads in the TERAS database (cf. Fig. S22 and S23) it becomes clear that only a few roads are detected, which are still interrupted and that many other lines exist which have to do with forest edges etc. Automatic line and roads detection is therefore for operational purposes not yet appropriate.

When multi-spectral data is used the spectral information can be used as an additional condition for the extraction and somewhat better results maybe expected. In case of microwave data the speckle hinders continuous edge detection so that more interruptions occur. Therefore a sufficient number of looks is necessary.



Figure S22: Lines automatically extracted from a SPOT-PAN image for the Heerde area.



Figure S23: Roads present in the TERAS database for the Heerde test area.

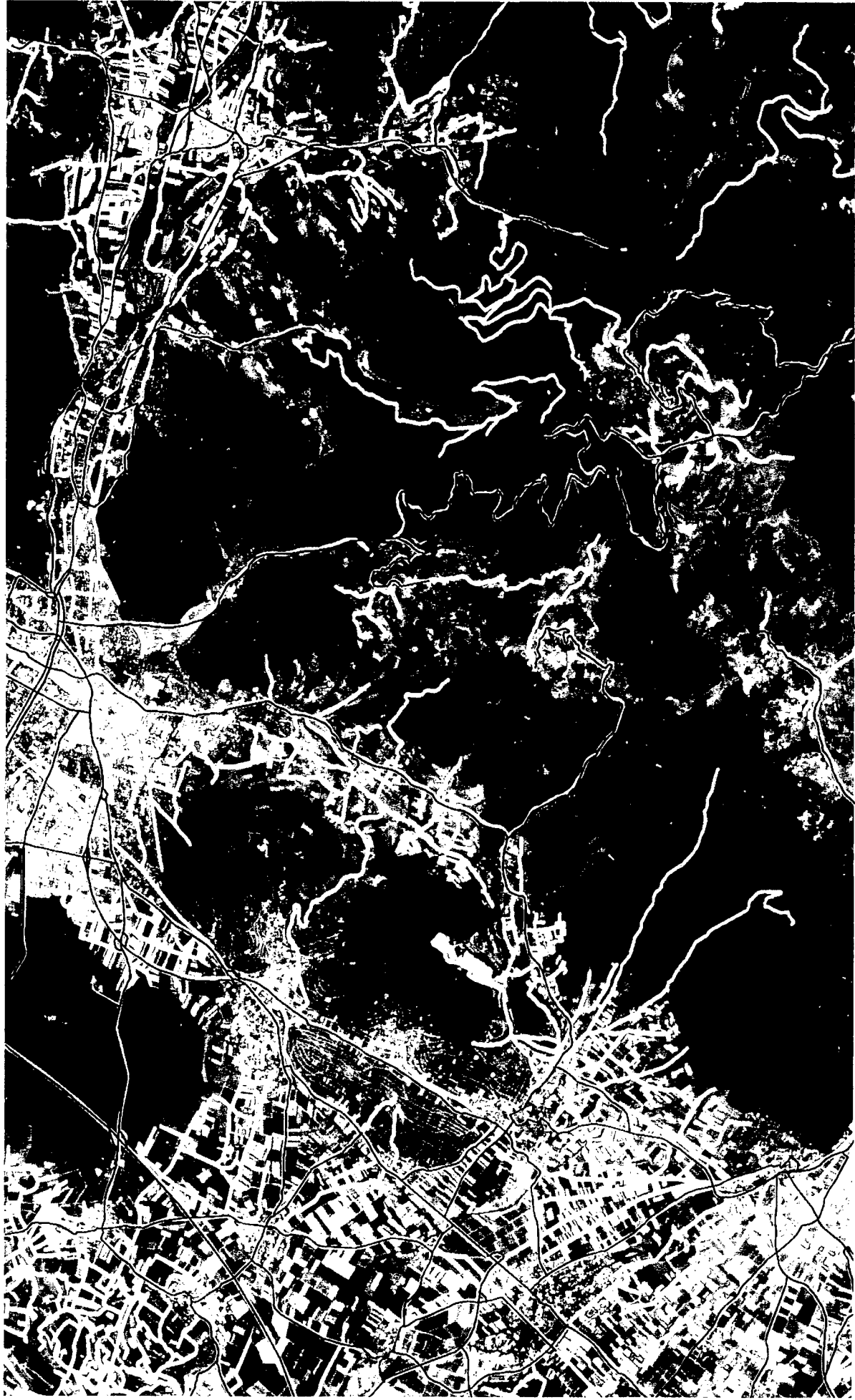
#### *Manual line extraction*

Manual line extraction is done by an interpreter who draws lines in an overlay from screen. The advantage is that the interpreter can prevent interruption and also can make decisions about the feature, whether a line is a road or a canal for example. Confusion can exist of course and the extracted product will always be approximate. In Fig. S24 we show roads extracted from a CAESAR image for the Heerde test area in an overlay on top of a SPOT image compared with all paved roads present in the 1:25,000 scale topographical map. Clearly almost all roads present on the topographical map are visible in the CAESAR images. Manual extraction of roads has been performed for most of the remote sensing images of the Heerde area and the results are shown and compared in Table 5 of the main report. For the Freiburg test area roads have been manually extracted and the results for the KVR image are compared with the roads present with the through roads present in the topographical map 1:50,000. This is shown in Fig S25 where the roads are shown in an overlay on top of a KVR image. Clearly many more roads are visible on the KVR image, probable often minor roads.



**Red: all paved roads from topographical map 1:25,000**  
**Yellow: extracted roads from CAESAR image**

72  
*Figure S24: Manually extracted roads for the Heerde test area in an overlay on top of a Spot-Pan image.*



**Red:** all through roads from topographical map 1:50,000  
**Yellow:** extracted roads from KVR image.

*Figure S25: Manually extracted roads for the Freiburg test area in an overlay on top of a KVR image.*

### S3.1.3 Point feature extraction

In a GIS database features are stored as points when the dimension of the feature is small for topographical purposes. These are most often buildings and other artificial features like bridges, high tension pylons etc. Whether they are seen in an image depends on the resolution, of course. We discuss here an extraction technique for point targets in microwave images.

In microwave images objects can be detected even when the resolution cell is larger than the object itself. This is due to specular or double bounce reflections which are often so strong that the reflection dominates the backscatter (i.e. the radiometric value) of the resolution cell.

Another property of microwave data is that these so-called point targets can quite easily be automatically extracted despite the presence of speckle. The statistics of the speckle is known and in a window moving over the image the central radiometric value with surrounding background values are compared. When the ratio between the central pixel value and the background value is high enough it can be said with more than 99 % confidence that the value is not due to speckle, but to a target showing a strong reflection. This means that we have detected a target. In Fig. S26 we give an example for an ERS image for the area near the village Olst. In the bottom panel we show the ERS image with yellow dots in overlay indicating detected targets. The same targets are overlaid on a KVR image, so that it is possible to identify the detected targets. Most of the targets are due to buildings, often farm houses. It is thus possible to detect objects as small as buildings in ERS images which on that scale hardly show any other details.



Figure S26: In the bottom an ERS image is shown with detected point targets (yellow dots). At the top a KVR image of the same area with the detected ERS point targets overlaid.

Another example of point target detection in microwave images is given by PHARS. In Fig. S27 we show an agricultural part of the Heerde test area where high tension pylons are indicated by a yellow outline. In the left panel a CAESAR image (1.5 m resolution) is shown with blue dots indicating the high tension pylons detected by PHARS as point targets. In the right panel the PHARS image of the same area is shown. In overlay the high backscatter levels are coloured. Note that the detected points are somewhat displaced from the high tension pylons seen in the CAESAR image. The displacement can be explained by the layover effect (see section S1.3.2) due to backscattered radiation from the top of the pylon. From the displacement the height of the pylon can be calculated, which appears to be 20 to 30 meter, quite in agreement with the expected height.

Note that the backscatter for some of the pylons is elongated. This is due to the fact that some pylons also give double bounce reflections, which are located at the pedestal of the pylon.

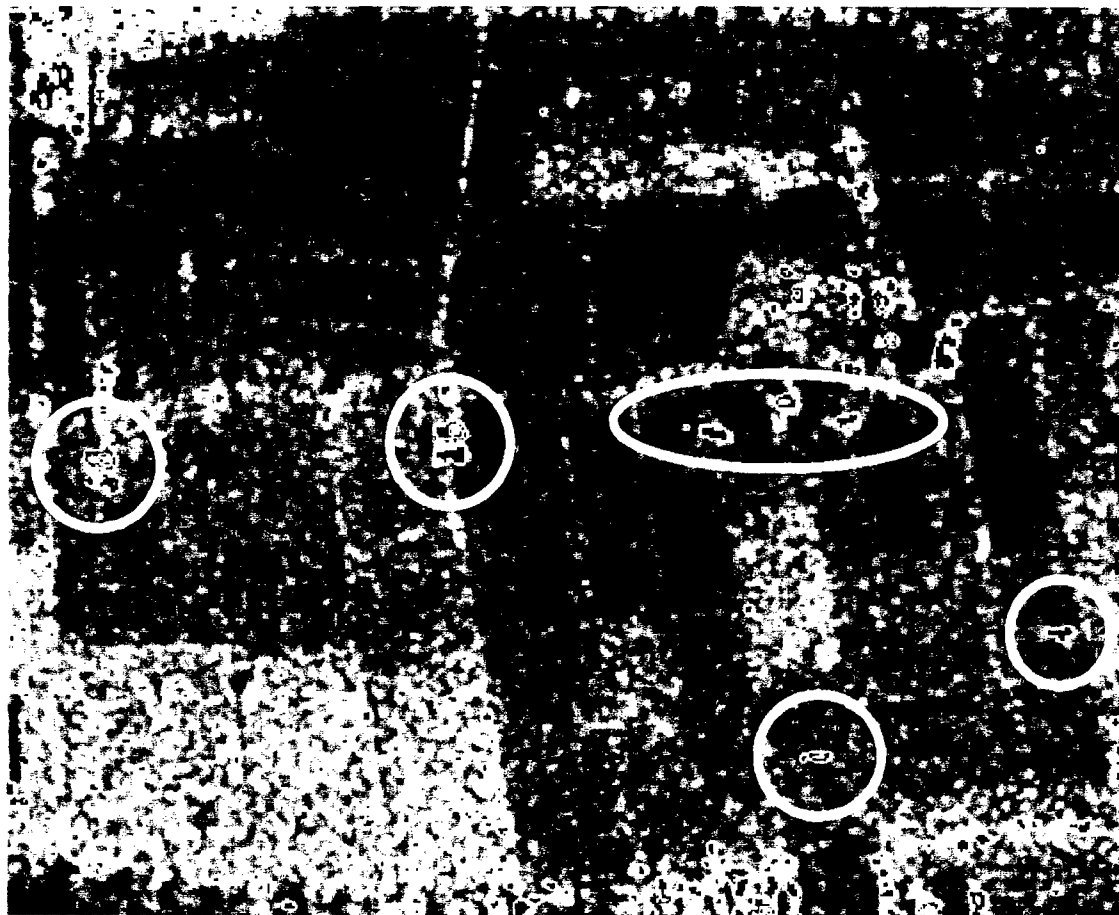


Figure S27: The Figure shows on the left a CAESAR image with high tension pylons detected by PHARS (blue dots). On the right the PHARS image is seen with high backscatter level in colour.

## S3.2 Height determination

### S3.2.1 Large scale height determination

#### *Optical stereo technique*

The principle of stereo-techniques for height determination is the same as the principle of 3-dimensional human observation. Because the same environment is observed from two different viewing directions, the elements at different distances from the observer do have different relative locations. The difference between the two locations (parallax) is a measure for the height or distance to the observer. When an object is observed not exactly perpendicular to the ground surface, the parts closer to the observer are displaced away from the image centre, as can be seen in Figure S28.

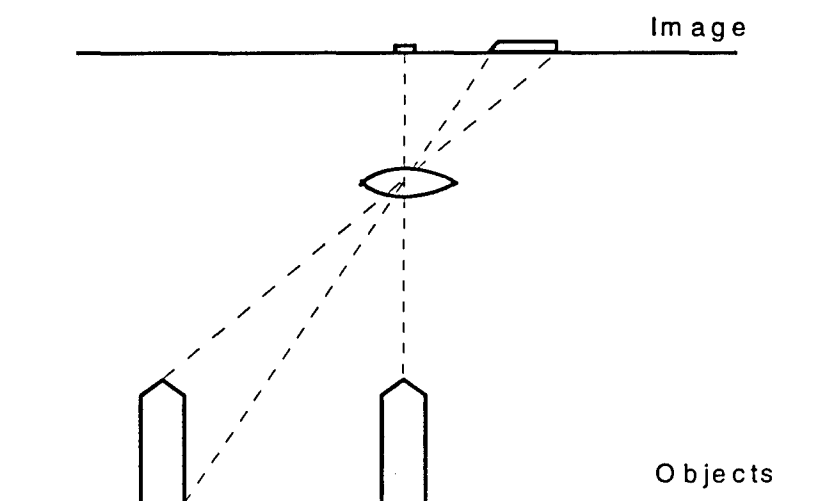


Figure S28: Displacement of high objects away from the image centre

Depending on the kind of projection system used, different types of displacement (parallax) are possible.

For photographs normally a camera system with a central projection is used. As a consequence of this the direction of the displacement is always away from the image centre. The viewing directions vary over the total image. For scanning systems with linear-arrays (pushbroom scanners) every line has its own projection centre situated in the middle of the line. So for a total image the displacement is always directed to the centreline (in flight direction) of the image. The viewing directions only vary in the image direction perpendicular to the flight direction. In case the scanning system is pointed forward in the flight direction also a (constant) displacement in the flight direction is generated.

Two images of the same area using different viewing directions are called stereo-pairs. From a stereo-pair height information can be extracted by measuring the parallaxes.

Different stereo-pairs are possible.

- Two overlapping photographs with central projection. This option is often used within the civil aerial photography.
- Two overlapping images of a pushbroom scanner taken from different viewing directions. For this option two configurations are possible.
  - 1) Along-track stereo: different viewing directions in flight direction.
  - 2) Across-track stereo: different viewing directions across flight direction.
 From an operational point of view the along-track stereo option is most favourable because the area is imaged within a very short time and within almost the same circumstances. For the across-track stereo option the area should be imaged again during a second overpass. This second overpass can be much later as a consequence of the required weather conditions etc., during which time the circumstances and also the object itself may be changed.

The different stereo-options are shown in Figure S29.

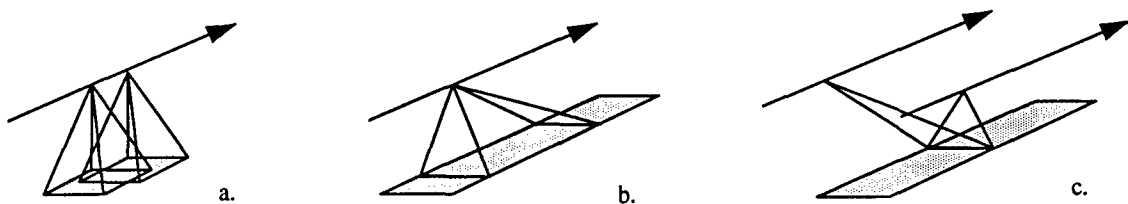


Figure S29: Overview of different stereo options: photographs with central projection (a), linescanners with along track stereo (b) and across track stereo (c)

Given the stereo-pair of images and the exact orientation parameters (position and attitude) of the images (or image-lines), corresponding points can be located and from the measured positions the heights can be computed. For the simple case of a point imaged on an image line from two viewing directions the following formula applies:

$$\delta H = \frac{\delta \text{pix} * p}{(B/H)}$$

where:

$\delta H$	=	difference in Height
$\delta \text{pix}$	=	difference in pixels (parallax)
$p$	=	pixelsize
$B$	=	Baseline length between the camera centres during image-acquisition
$H$	=	Height of the camera above the terrain during image-acquisition

As can be seen the accuracy of the height value depends on the pixelsize and on the value B/H, denoted as 'base to height ratio'. B/H is an important system parameter indicating the system geometry. B/H values of about 0.5 or larger give good results.

Methods for measuring three dimensional object coordinates:

The methodology for extracting height information from a stereo-pair of images is based on the knowledge of the geometry of the pair of stereo images (internal geometry of the sensor of one image, relative geometry of the sensors of the pair of images, absolute geometry of the sensors with respect to the earth) and the measurement of corresponding points in the separate images of the image pair. When the image coordinates of a certain point (object) can be measured in both images, and the geometry of the imaging systems during data acquisition is known, the coordinates of the object on earth can be determined. This can be done in several ways:

- Analogue using an analogue stereoplotter. This is a completely analogue instrument in which the two images can be rotated and translated with respect to each other so that the situation is obtained as during data acquisition. By mechanically manipulating two markers in the images, a stereo marker is obtained which can be placed on objects in the stereo image area. The coordinates of these objects in the terrain can be read out mechanically.
- Analytical using an analytical plotter. This is a semi-automated version of the analogue plotter. The geometrical computation process is performed by a computer instead of using sophisticated mechanical constructions. The measuring of the objects should still be done manually however.
- Fully automatic by using a digital plotter. In this case the images of the stereo pair are digitised (or acquired digitally) and the total process, both the geometric part and the object measuring part is performed by the computer. Only a human verification procedure is required.

Many optical sensor systems do have stereo capabilities. The third dimension in viewing the images provides valuable extra information for interpretation of the images and for generation of Digital Height Models or 3D datasets. In the tables of spaceborne and airborne optical sensor systems the possibility for stereo imaging is shown.

### *SPOT Stereo data processing and results*

#### SPOT stereo capabilities

As described in section S1.1.1 the SPOT system is a pushbroom line scanner which can point the sensor sideways across the track from -27 to +27 degrees. By using images of the same area which are sensed from two satellite tracks with different viewing directions a stereo dataset is obtained.

### SPOT data

The stereo dataset of Freiburg used for this project consists of three images:

1. Panchromatic, -29.6° 1994-07-02, 10.14h
2. Panchromatic, +00.2° 1994-08-04, 10.37h
3. Panchromatic, -25.5° 1991-08-06, 10.18h

With this dataset two stereo-pairs can be formed:

1. images from 02-07-94 and 04-08-94 with a time difference of 1 month and a viewing direction difference of 29.4 degrees. The time between the images is rather short and the B/H ratio 0.55, the image of 02-07-94 does have some clouds however.
2. images from 06-08-91 and 04-08-94 with a time difference of exactly 3 years and a viewing direction of 25.3 degrees. The time between the images is relatively long, but the season (and so light condition) is the same, the B/H ratio is some less 0.45, and both images do have no clouds.

### Method

There are several software packages which can automatically generate Digital Height Models out of optical stereo images. At NLR Erdas Orthomax is used. This software is capable of DEM generation out of aerial photographs (central projection) and SPOT stereo images (linear projection). The DEMs can have the format of a regular grid, or of a triangulated irregular network (TIN). The procedure of automatically generating DEM's using the Orthomax software package contains the following steps:

- Data pre-processing:
  1. Radiometric correction: suppression of image noise for a better matching procedure, stretching the image histogram for a better visual interpretation.
- Determination of the geometrical relation between the different images and the terrain:
  1. Internal orientation: determine the geometrical relation between the image and the sensor parameters;
  2. Relative orientation: determine the geometrical relation between the different images;
  3. External orientation: determine the geometrical relation between the images and the terrain coordinate system;
  4. Two or more images can be handled in parallel;
  5. Often estimated values for the position and attitude of the images are fed into the process. For SPOT these data are available in the SPOT header data;
  6. For the determination of the geometrical relation ground control points and tie points are measured in the images and in the terrain or in maps from the terrain;

7. Given the measurements, the estimated values for sensor orientation, position and optical characteristics, the optimal geometric system values can be determined by a computation process called triangulation.
- Image matching:
    1. The elevation model can be generated in a regular grid DEM or an irregular TIN.
    2. Automatic DEM generation by correlation techniques. This process can be steered by a number of parameters like thresholds for image noise and accuracy, grid resolution, number of image pyramid levels, interpolation techniques, and post-processing control parameters. The parameters depend on the image and sensor characteristics. A balance has to be found between enough accuracy of the found matches and minimising the unsuccessful matches.
    3. Manual correction in stereo environment: adaptation of wrong matched points and addition of break lines and characteristic points.

#### *Microwave stereo technique*

Like in the optical domain the stereo technique can also be applied to microwave imagery. It is also necessary to have two images from a different viewing point. Since the imaging geometry for microwave images is different from the optical the necessary conditions and starting-points for applying this technique are somewhat different.

The radar is always side looking so that no nadir images exist in the microwave domain. Therefore we have to combine images, which are looking from the same side (same-side stereo) or which are looking from the opposite (opposite-side stereo). For same-side stereo a look angle difference of about 15 degrees is usually optimal. In order to obtain the height information from a stereo pair, the two images have to be matched by correlating the images, which is hindered by speckle. Therefore the number of looks should not be too small.

#### *Interferometry*

As is explained in section S1.3.1 the phase difference between the pixels in the two images is used by this technique. The phase differences are created by combining (i.e. correlating) two images for which a slightly different position of the radar exist. These slightly different positions give different range distances to the terrain which also depends on the relief. The latter is the basis for retrieving the information about the relief, so that it is in principle possible to obtain a DEM of the terrain. Note that this type of correlating is different from the correlation which is mentioned above for the stereo technique. In this case the speckle does not hinder the correlation as long as viewing positions of the radar for the two images are almost exactly equal.

Two images of the same area using different viewing directions are called stereo-pairs. From a stereo-pair height information can be extracted by measuring the parallaxes.

Different stereo-pairs are possible.

- Two overlapping photographs with central projection. This option is often used within the civil aerial photography.
- Two overlapping images of a pushbroom scanner taken from different viewing directions. For this option two configurations are possible.
  - 1) Along-track stereo: different viewing directions in flight direction.
  - 2) Across-track stereo: different viewing directions across flight direction.
 From an operational point of view the along-track stereo option is most favourable because the area is imaged within a very short time and within almost the same circumstances. For the across-track stereo option the area should be imaged again during a second overpass. This second overpass can be much later as a consequence of the required weather conditions etc., during which time the circumstances and also the object itself may be changed.

The different stereo-options are shown in Figure S29.

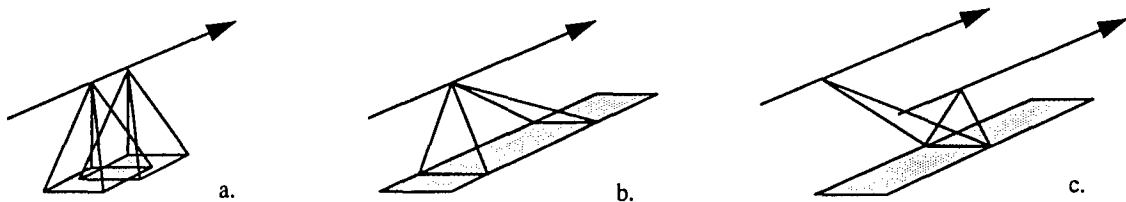


Figure S29: Overview of different stereo options: photographs with central projection (a), linescanners with along track stereo (b) and accross track stereo (c)

Given the stereo-pair of images and the exact orientation parameters (position and attitude) of the images (or image-lines), corresponding points can be located and from the measured positions the heights can be computed. For the simple case of a point imaged on an image line from two viewing directions the following formula applies:

$$\delta H = \frac{\delta \text{pix} * p}{(B/H)}$$

where:

$\delta H$	=	difference in Height
$\delta \text{pix}$	=	difference in pixels (parallax)
$p$	=	pixelsize
$B$	=	Baseline length between the camera centres during image-acquisition
$H$	=	Height of the camera above the terrain during image-acquisition

As can be seen the accuracy of the height value depends on the pixelsize and on the value  $B/H$ , denoted as 'base to height ratio'.  $B/H$  is an important system parameter indicating the system geometry.  $B/H$  values of about 0.5 or larger give good results.

Methods for measuring three dimensional object coordinates:

The methodology for extracting height information from a stereo-pair of images is based on the knowledge of the geometry of the pair of stereo images (internal geometry of the sensor of one image, relative geometry of the sensors of the pair of images, absolute geometry of the sensors with respect to the earth) and the measurement of corresponding points in the separate images of the image pair. When the image coordinates of a certain point (object) can be measured in both images, and the geometry of the imaging systems during data acquisition is known, the coordinates of the object on earth can be determined. This can be done in several ways:

- Analogue using an analogue stereoplotter. This is a completely analogue instrument in which the two images can be rotated and translated with respect to each other so that the situation is obtained as during data acquisition. By mechanically manipulating two markers in the images, a stereo marker is obtained which can be placed on objects in the stereo image area. The coordinates of these objects in the terrain then can be read out mechanically.
- Analytical using an analytical plotter. This is a semi-automated version of the analogue plotter. The geometrical computation process is performed by a computer instead of using sophisticated mechanical constructions. The measuring of the objects should still be done manually however.
- Fully automatic by using a digital plotter. In this case the images of the stereo pair are digitised (or acquired digitally) and the total process, both the geometric part and the object measuring part is performed by the computer. Only a human verification procedure is required.

Many optical sensor systems do have stereo capabilities. The third dimension in viewing the images provides valuable extra information for interpretation of the images and for generation of Digital Height Models or 3D datasets. In the tables of spaceborne and airborne optical sensor systems the possibility for stereo imaging is shown.

### *SPOT Stereo data processing and results*

#### SPOT stereo capabilities

As described in section S1.1.1 the SPOT system is a pushbroom line scanner which can point the sensor sideways across the track from  $-27$  to  $+27$  degrees. By using images of the same area which are sensed from two satellite tracks with different viewing directions a stereo dataset is obtained.

### SPOT data

The stereo dataset of Freiburg used for this project consists of three images:

1. Panchromatic,  $-29.6^\circ$  1994-07-02, 10.14h
2. Panchromatic,  $+00.2^\circ$  1994-08-04, 10.37h
3. Panchromatic,  $-25.5^\circ$  1991-08-06, 10.18h

With this dataset two stereo-pairs can be formed:

1. images from 02-07-94 and 04-08-94 with a time difference of 1 month and a viewing direction difference of 29.4 degrees. The time between the images is rather short and the B/H ratio 0.55, the image of 02-07-94 does have some clouds however.
2. images from 06-08-91 and 04-08-94 with a time difference of exactly 3 years and a viewing direction of 25.3 degrees. The time between the images is relatively long, but the season (and so light condition) is the same, the B/H ratio is some less 0.45, and both images do have no clouds.

### Method

There are several software packages which can automatically generate Digital Height Models out of optical stereo images. At NLR Erdas Orthomax is used. This software is capable of DEM generation out of aerial photographs (central projection) and SPOT stereo images (linear projection). The DEMs can have the format of a regular grid, or of a triangulated irregular network (TIN). The procedure of automatically generating DEM's using the Orthomax software package contains the following steps:

- Data pre-processing:
  1. Radiometric correction: suppression of image noise for a better matching procedure, stretching the image histogram for a better visual interpretation.
- Determination of the geometrical relation between the different images and the terrain:
  1. Internal orientation: determine the geometrical relation between the image and the sensor parameters;
  2. Relative orientation: determine the geometrical relation between the different images;
  3. External orientation: determine the geometrical relation between the images and the terrain coordinate system;
  4. Two or more images can be handled in parallel;
  5. Often estimated values for the position and attitude of the images are fed into the process. For SPOT these data are available in the SPOT header data;
  6. For the determination of the geometrical relation ground control points and tie points are measured in the images and in the terrain or in maps from the terrain;

7. Given the measurements, the estimated values for sensor orientation, position and optical characteristics, the optimal geometric system values can be determined by a computation process called triangulation.
- Image matching:
    1. The elevation model can be generated in a regular grid DEM or an irregular TIN.
    2. Automatic DEM generation by correlation techniques. This process can be steered by a number of parameters like thresholds for image noise and accuracy, grid resolution, number of image pyramid levels, interpolation techniques, and post-processing control parameters. The parameters depend on the image and sensor characteristics. A balance has to be found between enough accuracy of the found matches and minimising the unsuccessful matches.
    3. Manual correction in stereo environment: adaptation of wrong matched points and addition of break lines and characteristic points.

#### *Microwave stereo technique*

Like in the optical domain the stereo technique can also be applied to microwave imagery. It is also necessary to have two images from a different viewing point. Since the imaging geometry for microwave images is different from the optical the necessary conditions and starting-points for applying this technique are somewhat different.

The radar is always side looking so that no nadir images exist in the microwave domain. Therefore we have to combine images, which are looking from the same side (same-side stereo) or which are looking from the opposite (opposite-side stereo). For same-side stereo a look angle difference of about 15 degrees is usually optimal. In order to obtain the height information from a stereo pair, the two images have to be matched by correlating the images, which is hindered by speckle. Therefore the number of looks should not be too small.

#### *Interferometry*

As is explained in section S1.3.1 the phase difference between the pixels in the two images is used by this technique. The phase differences are created by combining (i.e. correlating) two images for which a slightly different position of the radar exist. These slightly different positions give different range distances to the terrain which also depends on the relief. The latter is the basis for retrieving the information about the relief, so that it is in principle possible to obtain a DEM of the terrain. Note that this type of correlating is different from the correlation which is mentioned above for the stereo technique. In this case the speckle does not hinder the correlation as long as viewing positions of the radar for the two images are almost exactly equal.

For applying this technique it is necessary that the phase differences over the image show an interference pattern. Generally when the distance between the two radars is not too large (look angle difference smaller than 0.1 degree) and when the images are recorded simultaneously (single pass interferometry) this is the case. The images are then said to be correlated.

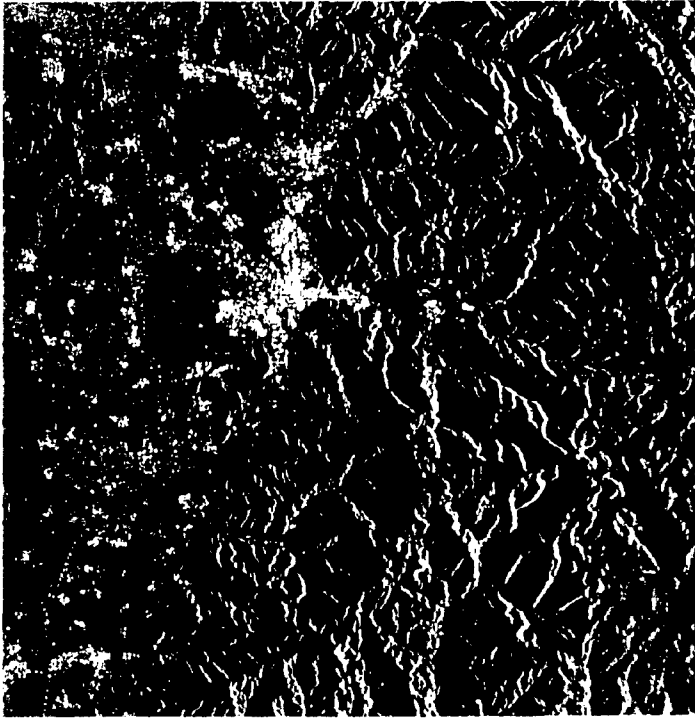
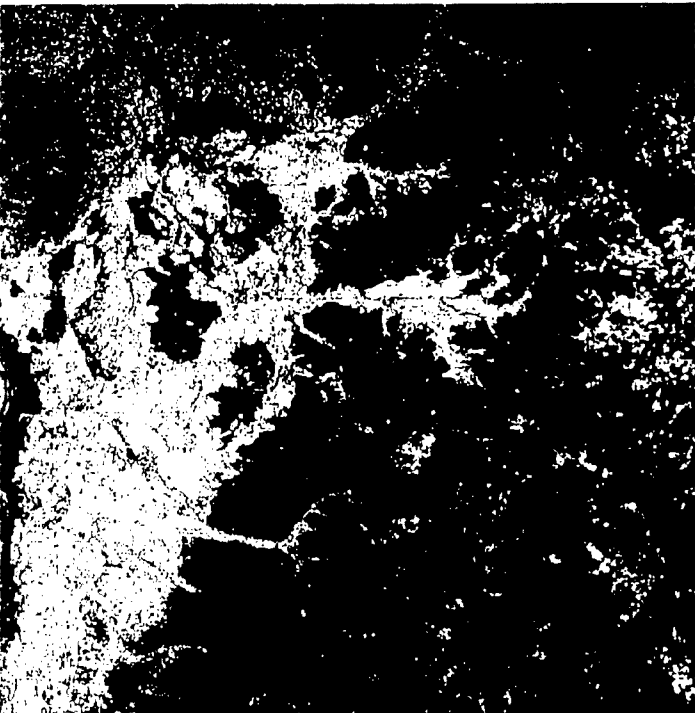
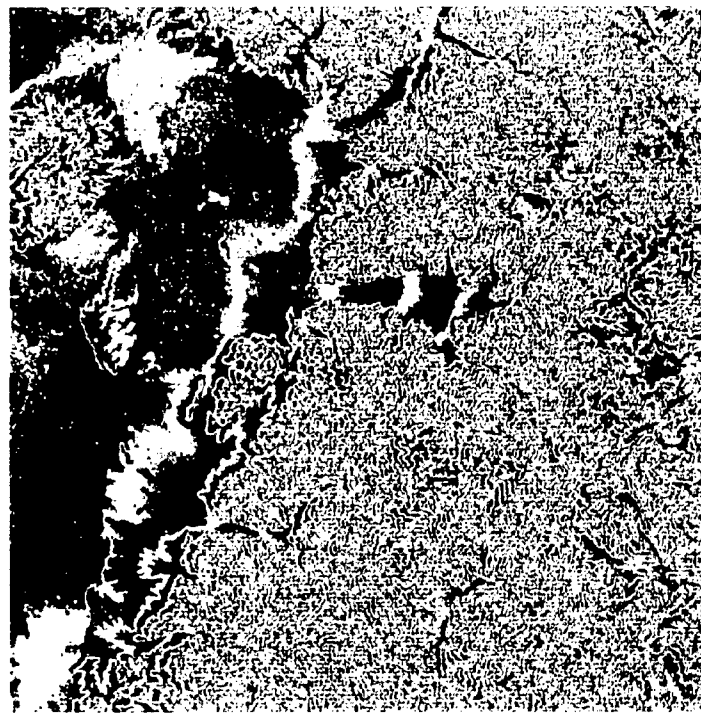
When two images are combined from different viewing positions no correlation (sometimes also called the coherency) can be expected so that the interferogram only shows noise. This is the case when ascending and descending ERS images are combined for example.

Also when two images with almost the same viewing position but recorded at different times (repeat pass interferometry) are combined, decorrelation can be expected when the terrain has changed. These changes can be small but are apparent for the radar when they influence the backscatter. For example when the surface is covered with snow or not causes decorrelation. Vegetation causes decorrelation when the leaves, important for the backscatter, change their positions due to wind. Also water surfaces are always decorrelated since the waves change very rapidly.

With the ERS satellite it is possible to obtain images from almost exactly the same viewing position. Typical baselines, which is this distance between the parallel orbits, are in the order 1 km.

The revisit time for ERS is several weeks and it appears that most vegetated surfaces are decorrelated then so that no DEM could be acquired except for very dry areas (e.g mountainous areas of Sicily).

Due the launch of the ERS-2 satellite it was possible to obtain ERS-1 and ERS-2 images from the same area and same viewing position, and only one day apart. These data has also been obtained for testsite Freiburg. In order assess to potential for height derivation we have created from this pair of images a correlation (coherence) image and an interferogram (phase difference image). We show these images in Fig S30, together with an average backscatter image and a DEM (DTED).

**Backscatter****Shaded elevation model****Coherence****Phase difference**

*Figure S30: The figure shows an average backscatter image (top left), a coherence image (bottom left) and phase difference image with fringes (bottom right) for test site Freiburg. Also a shaded elevation model (top right) is shown.*

From the images it is clear that in the Rhine valley and in the dales the correlation or coherence is high (bright in the coherence image), so that phase differences and height information can be obtained. The phase differences in the phase image are coloured and show a cyclic pattern (so-called fringes). The height difference between two successive fringes is about 70 m. The actual area where significant relief is present is covered with forest and the coherence is low (dark in the coherence image). As a consequence the phase image is noisy implying that no height information can be extracted.

We conclude therefore that in this case and for forested areas in general repeat pass interferometry is not well able to produce a DEM. In order to do this single pass interferometry is needed which is not yet available from space. An experiment with single pass interferometry using the space shuttle is planned around the year 2000. Airborne single pass interferometry is already possible, but is more applicable to the determination of small scale relief (see section S3.2.2), seen the smaller swath and higher resolution.

### **S3.2.2 Small scale height determination**

#### *Optical shadow method*

Within optical images the height of objects can be observed indirectly by shadows of the objects on the ground. For optical images the shadow is caused by the sun illumination.

The size of the shadow, and related to it the accuracy of the object-height, depends on the incidence angle of the sun illumination (i.e. the angle between the vertical and the incident radiation). This angle depends on:

- The time of the year. The latitude position of the sun relative to the earth varies over the year between the two tropics ("keerkringen") at  $-23.5^\circ$  and  $+23.5^\circ$  latitude.
- The latitude position on earth. The further the position on earth is located from the latitude of the sun, the larger is the nadir angle of the sun in north-south direction.
- The time of the day. During the day the earth moves relative to the sun in east-west direction. At 12:00 o'clock solar time the sun is at its highest position of the day. The longer away from this time, the larger the sun nadir angle in east-west direction will be.

For the Dutch situation (latitude  $52^\circ$ ) the nadir angle of the sun at noon in north-south direction varies between 15 and 60 degrees over the year. The incidence angle should not exceed 70 degrees or so since then the shadows hinder the interpretation of the image.

There is a simple relation between the incidence angle of the sun, the object height and the shadow length.

$$\text{Height} = \text{Length of shadow}/\tan(i)$$

where the  $i$  is the incidence angle. If the shadow length can be measured with an accuracy of half a pixel, then the accuracy of the height is:

$$\delta\text{Height} = \delta\text{Length of shadow}/\tan(i) = 0.5 * \text{pixelsize}/\tan(i)$$

In the table below the height accuracy is given for images with a pixelsize of 1.5, 3 and 10 meter:

$\delta$ Height for various angle and pixelsizes

angle $i$	$\tan(i)$	1.5 m	3 m	10 m
70	0.36	0.5	1.1	3.6
60	0.57	0.9	1.8	5.7
50	0.84	1.2	2.5	8.4
40	1.19	1.8	3.6	11.9
30	1.73	2.6	5.2	17.3
20	2.75	4.1	8.2	27.5

An experiment has been done with CAESAR and SPOT images. In order to measure the shadow lengths, the images were rotated over the sun zenith angle so that the shadows in the image were directed exactly horizontal. Secondly the shadows were determined by using one of the components of the with the principal component algorithm transformed image. With a special programme the shadow lengths were measured, and with the parameters of the sun position the heights of the startpoints of the shadows were computed. The heights were visualised in a separate image by giving the start pixels of the shadows a red colour with the intensity corresponding to the computed height values. The result is shown in Figure S31.

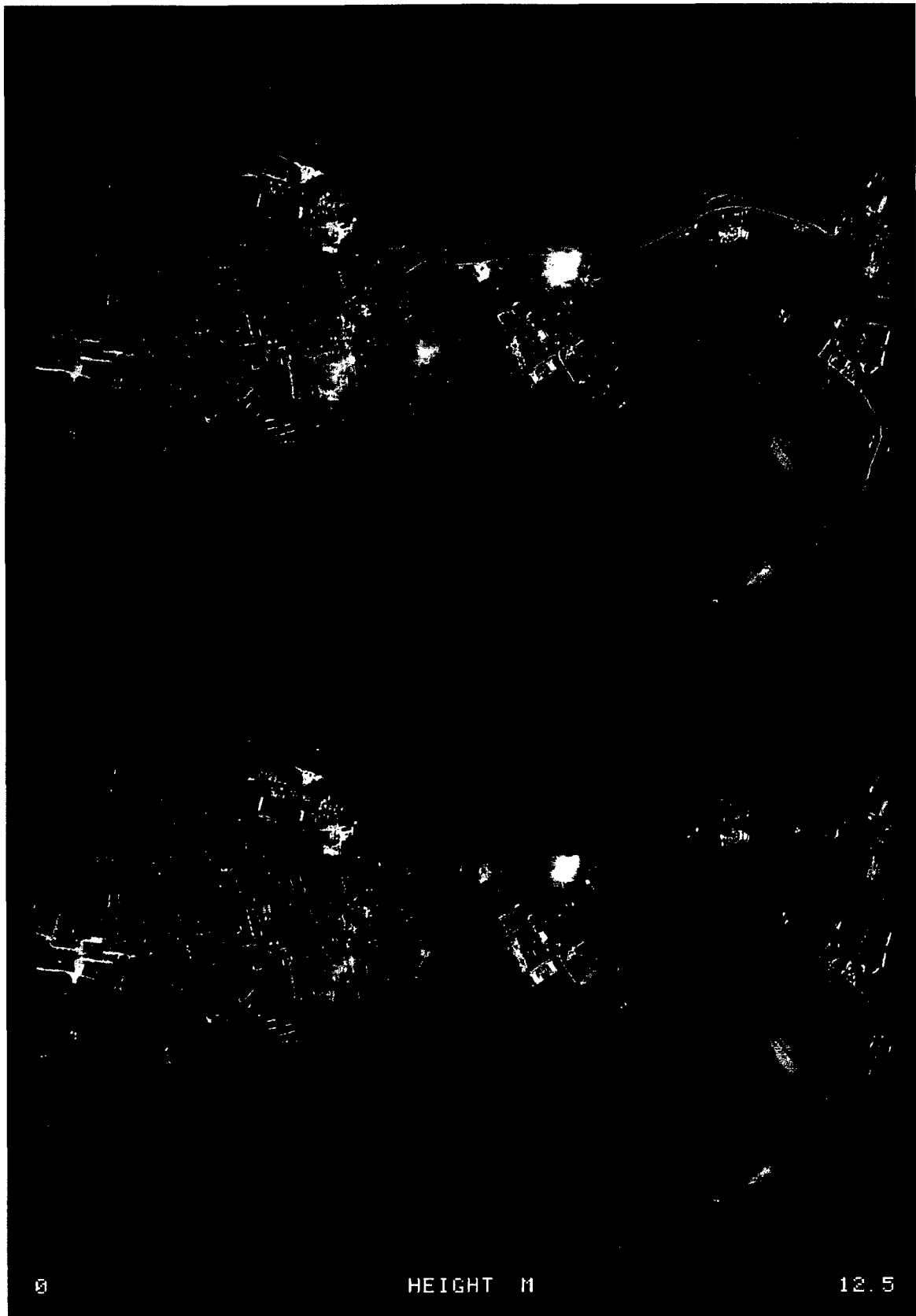


Figure S31: Figure showing height determination in CAESAR images using shadow.

### *Microwave shadow method*

Like in the optical domain shadows in the image can be used to obtain the height of the objects. Since microwave images are obtained by receiving radiation from an active source where receiving and transmitting occurs at the same place shadowing is always aligned in range direction. Since also the local incidence angle is known the height determination using shadowing with microwave images is more simple than with optical imagery and it is possible to automatically determine height values.. Abovementioned equations for the retrieval of the height and accuracy in the optical are also applicable in the microwave. Pixelsize, however, should be replaced by the dimension of the resolution cell.

Using PHARS data of a part of testsite Heerde we have developed an automatic procedure for determining the height. A shadow feature is characterised by a sharp edge from bright to an elongated dark patch.

By detecting this sharp edge and by determining the length of the dark patch in range direction the height can be calculated.

In Figure S32 we show PHARS data of a part of the Heerde test area with forested areas and arable land (top). The bottom picture shows a so-called derivative image where the bright parts mark the sharp edges.

By taking the bright values of this latter image above a certain threshold and under the condition that the dark patch in the original backscatter images is below a certain threshold the height is calculated and stored in a GIS database. The points for which the height is calculated are shown as yellow dots in an overlay on the backscatter image. In a GIS environment (ERDAS or ArcInfo) clicking on these points would give the height in meters as return. Since the resolution of the system is about 6 meter and the incidence angle is about 60 degrees the accuracy of the height determination is about 3 to 4 meter.

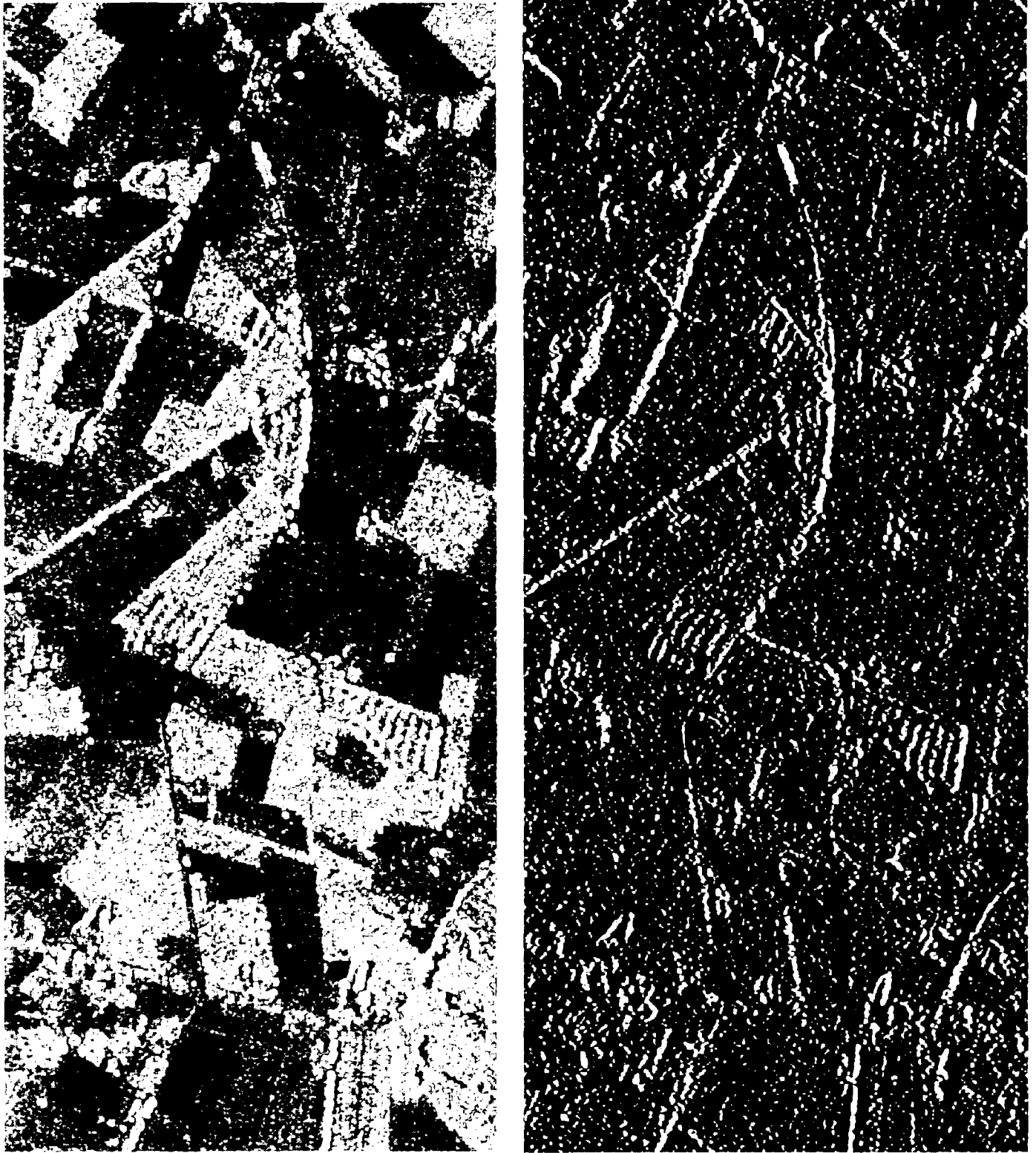


Figure S32: PHARS image showing points where the height has been calculated from the shadow (top). At the bottom a 'derivative image' is showing the edges as bright parts.

### *Stereo technique*

In order to retrieve small scale height variation the resolution of the determined DEM should be high enough. This means that the resolution of the system should be high enough since the resolution on the height measurement is related to the geometrical resolution (see equations). In practice this means that airborne sensors have to be used. We describe here the stereo capability of CAESAR as example.

#### CAESAR stereo capabilities

The CAESAR system does have along-track stereo capabilities (see for a general description of CAESAR (section S1.1.3). The information of channels with different viewing directions can be used to derive height information of the terrain. Using a combination of a backward and forward looking channel (-11.5 and +11.5 degrees) a Base to Height ratio (B/H) of 0.41 is obtained. A central channel in combination with a forward or backward channel results in a B/H ratio of 0.20. Also combinations between a channel of the forward looking camera and a downlooking camera can be used resulting in B/H ratios of up to 1.7. In practice up to now the three channels of one downlooking camera are used, resulting in B/H ratios of 0.41 and 0.20. Using CAESAR data with a resolution of 0.5 meter theoretically a height accuracy of about 35 cm can be reached. In practice this accuracy is expected to be in the order of one meter, because of the less accurate flight parameters.

#### Method

In order to automatically generate a Digital Elevation Model from the CAESAR stereo images NLR in cooperation with DUT Faculty of Geodesy are developing the CAEDEM software (CAESAR Digital Elevation Modelling). This package can be divided into two elements:

1. Generation of a set of corresponding image points in two (or more) stereographic images;
2. Computing the position and elevation values for the corresponding image point, using a geometric model and flight data.

#### Results

No CAESAR stereo dataprocessing was performed within this project, because of two reasons. Firstly the CAESAR data as used within this project were not acquired in stereo and secondly the CAEDEM software is not in an operational stage at this moment. In order to give an impression of the CAESAR stereo capabilities a stereo image represented in anaglyph colours of a part of the airbase Soesterberg is shown in Figure S33.



Figure S33: Stereo image of part of Airbase Soesterberg represented in anaglyph colours. Spatial resolution 0.5 meter, B/H 0.41. Special red/green glasses are required to interpret this image.

### *Interferometry*

As was explained in section S3.2.1 single pass interferometry using two microwave images obtained at the same time, but from slight different positions can be used to determine the terrain height. Especially images from airborne interferometric systems are suitable for the determination of small scale height variations and the height of objects in the terrain because of the high resolution. For the Heerde area we have obtained airborne interferometric data from the DRA C-band SAR. In this system two antenna's are used about 1.8 m apart (vertical baseline), which results in an incidence angle difference of 0.03 degrees at the flying height of 1.5 km. Because of this small angle and because the images were recorded at the same time no decorrelation is expected, so that the phase image should show clear fringes without noise. In Fig. S34 we show at the bottom the phase images. The patterns show dips due to the movements of the plane. Note that noise is seen in the phase images when the plane is moving. Since the DRA-SAR is an experimental system no correction for plane movements (motion compensation) has been applied, which has a negative effect on the accuracy of the height determination. This is contrary to the situation for PHARS and PHARUS where the plane movement is recorded, so that the imagery can be corrected for plane movements.

In the phase images also smaller 'disturbances' which contain the actual height information, are visible. The derived height after motion compensation and interferometric processing is shown in an overlay on top of the SAR image. Height levels below 5 meter are made transparent while height levels above 5 meter are in colour. The height determination for this area are mainly of trees, but for other areas the height of taluds, hill etc., can be determined as well with this technique.

# Interferometric height determination

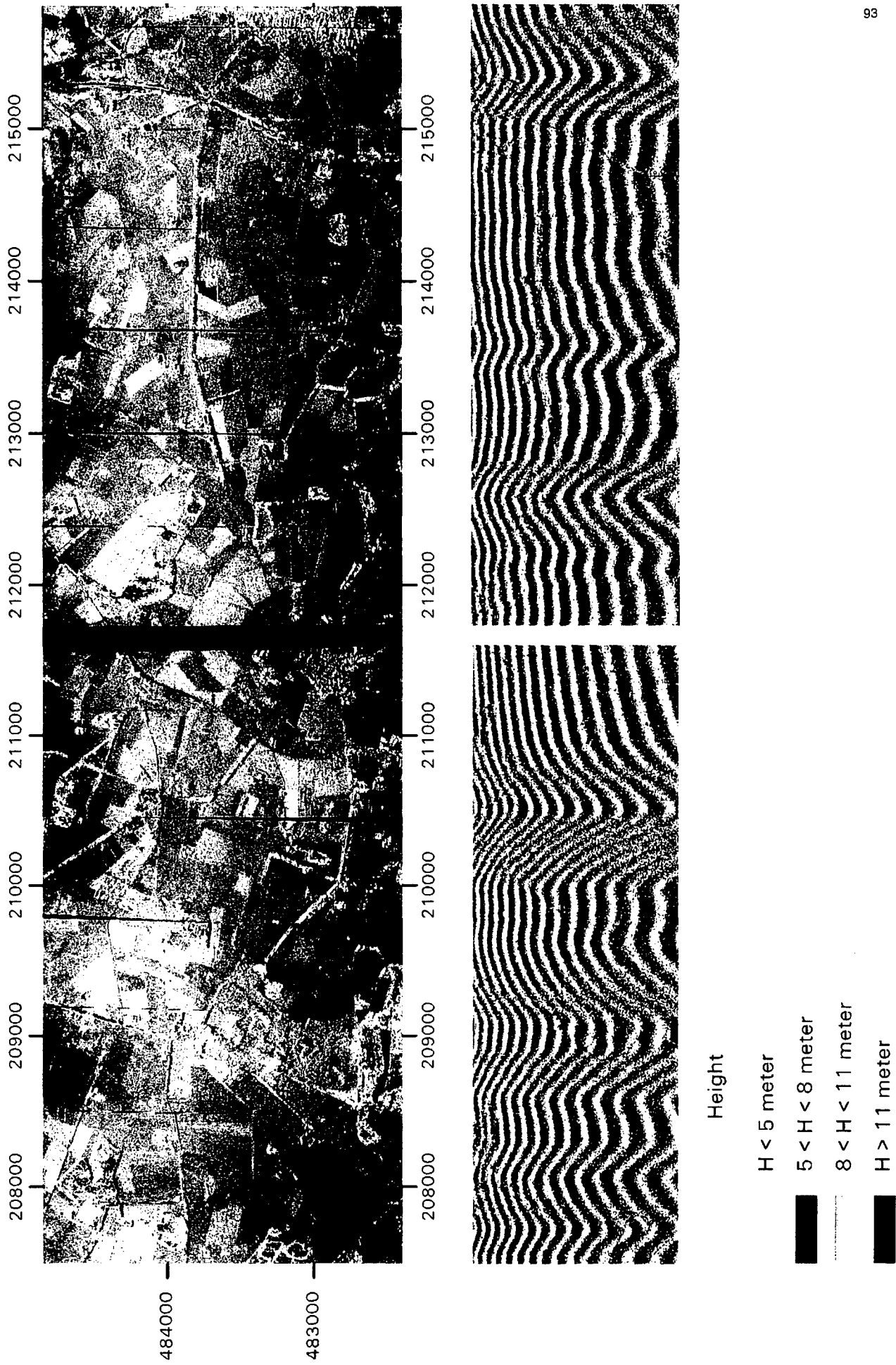


Figure S34: Single pass airborne interferometric height determination. See text for explanation.

### S3.3 Multitemporal analysis

#### *Optical*

To monitor changes, which have taken place in an area during a specific time, a very commonly used method is to compare remote sensing images of different dates. This method is often called multitemporal analysis. Before the comparison can be made it is necessary to georeference the various satellite and airborne images into the same coordinate system.

In the present study, three images were selected for analysing the changes that have taken place in the spatial distribution of water features in the IJssel area near Diepenveen.

The following images were used:

- CAESAR                    22 September 1994      3 metre resolution
- Landsat TM                18 October 1993        30 metre resolution
- SPOT XS                    10 June 1992            20 metre resolution

In order to extract the water features from the images, only the near infrared channel is used because in this channel the best distinction can be made between water and land. A straightforward linear contrast stretch is sufficient to derive images in which the water is mapped to the colour white and the land is mapped to the colour black. This was done for each separate image.

Black and white 'water/land' images can now be compared by combining them into a new, 3-channel, file. For example, in this new file, the 1994 image is assigned to the colour red, the 1993 image to the colour green and the 1992 image to the colour blue. The resulting file shows all occurring changes between the three years, however experience learns that the information is often too complex for a proper interpretation.

Therefore, instead of three, two years are combined for comparison which makes interpretation easier. The most recent year gets the colour red and the previous year gets the colour cyan (green and blue). Three, so-called, change images were made from the years 1994+1993, 1993+1992 and 1994+1992.

Fig. S35 shows in the right column the three change images while in the left column the same area is enlarged and added by a shaded topographic map to improve the recognition of the location. The areas that appear white have got the same (high) contribution of red and cyan; these are areas where no changes took place. In the 1994/1993 image, also cyan areas can be recognised in the IJssel river area indicating that there were high water levels in 1993 while the area was not flooded in 1994. Near the railway (Hengforden), two small red spots can be recognised; these are sand pits which have been dug after 18-10-93.

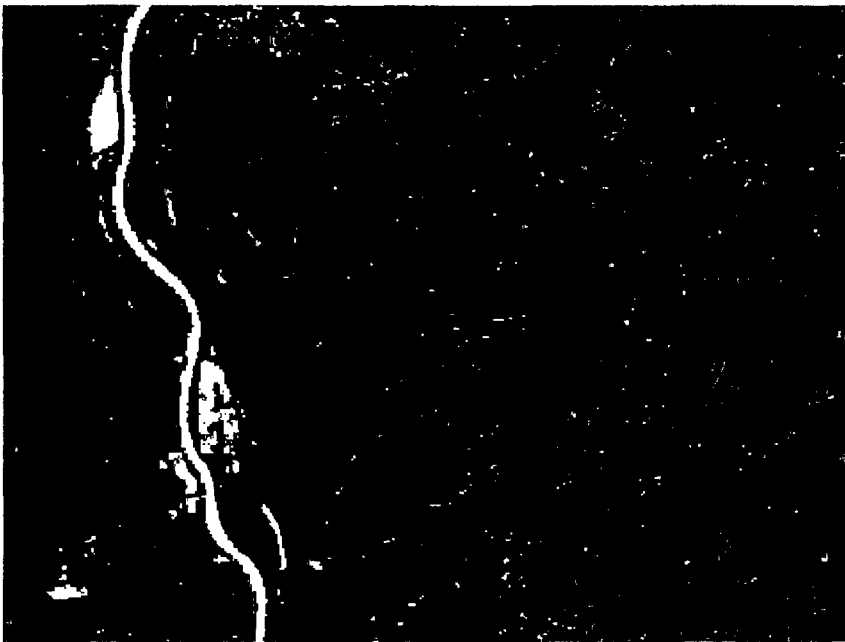
Not only water features are shown in the change imagery. For the wooden areas in the East, red and cyan colours indicate shadow effects from trees. The vertical red bar in the south of the area was not recorded by the CAESAR scanner.

# Multitemporal analysis on water



Change detection between 1994 and 1993

In red : Caesar 22-9-94  
In cyan : Landsat TM 18-10-93



Change detection between 1993 and 1992

In red : Landsat TM 18-10-93  
In cyan : Spot XS 10-6-92



Change detection between 1994 and 1992

In red : Caesar 22-9-94  
In cyan : Spot XS 10-6-92

Figure S35: Detected changes in an overlays on top of a topographical map. See text for further explanation.

### *Microwave*

Since microwave imaging is weather independent collection of images over certain time intervals can be ensured. These advantages make that change detection with microwave is relatively easy.

We present here an example (see Fig. S36) for the city of Zwolle, where two image from the ERS satellite in 1991 and 1992 are compared. One image is shown in the colour cyan and the other in red, so that when no changes are present a grey tone is seen, while when changes are present red or cyan colours are seen. The most prominent changes are selected and shown in an overlay on top of a SPOT image of 1992. The significant changes detected here are a new urban part and a sporting complex built between 1991 and 1992 (big red areas in the lower part of the image).

## Change detection with ERS (Zwolle)



**ERS 1991 (cyan) and ERS 1992 (red)**



**Spot image with detected changes**

*Figure S36: ERS images from 1991 (cyan) and from 1992 (red) of the city Zwolle (left). Significant changes are shown in overlay on top of a Spot-Par image.*



## S4. Sensor and data fusion

Sensor fusion or data fusion is called the procedure to obtain information by using more than one sensor. It is clear that different sensors providing additional and independent information about an object or feature offer a more complete picture of what is going on. For example the recognition of an power plant is facilitated when the three different wavelength regions used:

1. optical imagery shows a large complex near a river or lake.
2. thermal infrared imagery shows the presence of excess heat by detecting the warm cooling water.
3. microwave imagery shows a collection of point targets indicating high structures like pipes, tanks etc.

A practical way of data fusion from e.g. sensors in different wavelength domain is to combine images from the different type of sensors in the three colour channels. We give here two examples where we have combined CAESAR data with PHARS and TIR data.

Since channels 1 and 2 for CAESAR are rather correlated a CAESAR image (RGB: band 3,2,1) shows cyan tints, except for vegetated parts which are reddish. By changing either band 1 or 2 for a TIR or PHARS image in a RGB colour composite we obtain images with more variation in colours. This is due to the fact that TIR or PHARS images contain information which is independent from the optical data. It is clear that by observing more colour tints in the displayed image more information can be retrieved during the interpretation.

In Fig. S37 a colour composite with CAESAR and TIR are shown at the bottom. In this Figure it is now possible to discriminate easier between houses, streets and fields. The houses and buildings are coloured red (TIR is displayed in the red channel), since they are warm, while the streets are blue/purple, while they are cooler but have a high reflectivity (CAESAR band 2 is displayed in the green channel). The fields are greenish since they have a high reflectivity in band 3 (green channel) of CAESAR.



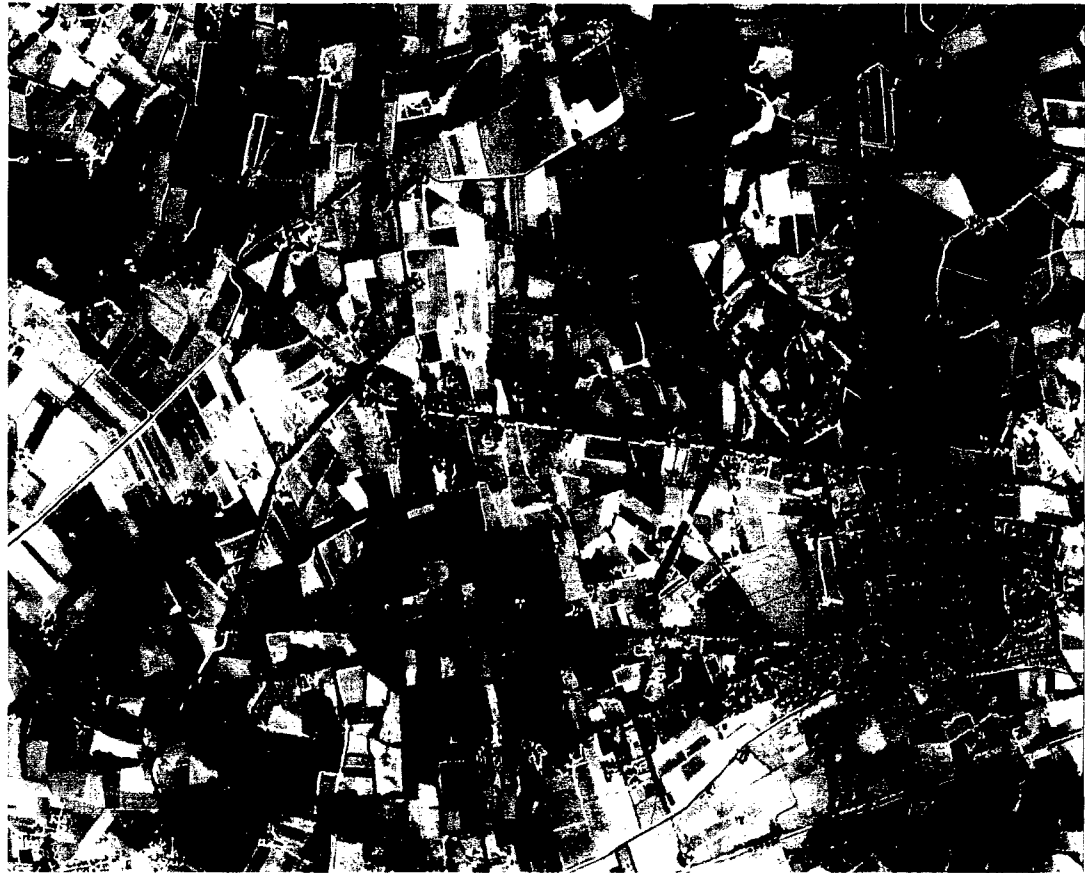
**CAESAR RGB: band 3,2,1**



**TIR (R) AND CAESAR (GB: band 3,1)**

*Figure S37: Figure showing sensor fusion between CAESAR and TIR images (bottom) compared with false colour image of CAESAR (top) for the area near the village Olst.*

In Fig. S38 PHARS data (blue channel) is combined with CAESAR data (band 3 and 2 in the green and red channel, respectively). The forest and fields show more contrast in the microwave, because the microwave radiation is more intensively scattered by a thick vegetation layer (forest) than a small layer (e.g. grass), while the reflectivity for vegetated surfaces does not vary that much in the optical. Therefore the forest is coloured blue, since the microwave dominates, while grass is coloured green, since the reflected radiation dominates in the NIR dominates. For maize the situation is in between and maize fields are coloured light blue.



**CAESAR (RGB: band 3,2,1)**



**CAESAR (RG: band 2,3) and PHARS (B)**

Figure S38: Figure showing sensor fusion between CAESAR and PHARS images (right), compared with a false colour image of CAESAR (top) for the area near the village Diepenveen.

Sensor fusion only works well when the quality of the data from the different sensors is comparable. To retrieve more information about a geographical feature with sensor fusion all used sensors should be able to see (i.e. to detect) the feature. The ability to detect features is summarised in Table 4 in section 4.4 (main report) for the various sensors.

We have given here two examples of data fusion, where the images are fused before the desired information is extracted. This is a direct way of data fusion where the data is combined using several techniques: e.g. false colour imaging, colour transformations, principle component analysis et cetera.

Another way of fusion is to combine information extracted from the separate images, e.g. in a geographical information system:

Summarising we can therefore discriminate between two ways of fusion.

- 1) Data fusion: the fusion takes place before information is extracted.
- 2) Information fusion: information is extracted from the separate images and is fused afterwards.

## Distributielijst

1. DWOO
2. HWO-KM\*
3. HWO-KL
4. HWO-KLu\*
5. HWO-CO\*
6. KMA, t.a.v. Ir. J. Rogge
7. DM&P TNO-DO
8. Directeur TNO-PML\*
9. Directeur TNO-TM\*
10. Accountcoördinator KL\*
- 11 t/m 13. Bibliotheek KMA
14. HQ 1 (GE/NL) Corps G-2 Division (MilGeo), NL Topo Offr
15. Staf 1 (NL) Divisie H-Sie G2
16. C-101 MI peloton
17. Wing Mission Planning Vlb. Volkel, Maj. J.W. van den Heuvel
18. Chef der Hydrografie, G. Spoelstra
19. Militaire Inlichtingendienst, Afd. Inl., Dr. L.H.P. Meijer
20. Genie OC, Hfd Kenniscentrum
21. KMA, Ir. J. Schellekens
22. NLR, Ir. M. van Persie
23. NLR, Ing. H.H.S. Noorbergen
24. NLR, Dr. G. van den Burg
25. TDN, Ir. P. van Asperen
26. TDN, Ir. E. Kolk
27. LAS/BO/OB, Lkol. A. Dondorp
28. DMKL/T&WO, Ir. N Pos
29. DMKM/WCS/COSPON, Drs. W. Pelt
30. DOPKLu, Ir. S.J.J. de Bruin
31. DMKLu/MXS, Ir. G. de Wilde
32. MID-KL, bureau MilGeo, Maj. A. Schoonderbeek
33. MID-KL, bureau MilGeo, Maj. R.J.T. Veltman
34. MID-KL, bureau MilGeo, Kap. G.L. Weerd
35. OCEDE/KCEN/SMID, Hfd sectie plannen, Lkol. G.F. van Kempen
36. OCEDE/KCEN/SMID, Maj. M. van Ommen Kloeke
37. OCEDE/KCEN/SMID, H. Ebbers
38. Directeur TNO-FEL
39. Adjunct-directeur TNO-FEL, daarna reserve
40. Archief TNO-FEL, in bruikleen aan MPC\*
41. Archief TNO-FEL, in bruikleen aan Accountmanager KL\*
42. Archief TNO-FEL, in bruikleen aan Ir. P. Hoogeboom
43. Archief TNO-FEL, in bruikleen aan Dr. A.C. van den Broek
44. Archief TNO-FEL, in bruikleen aan Dr.ir. G.J. Rijckenberg
45. Archief TNO-FEL, in bruikleen aan Ir. P.J. Schulein
46. Archief TNO-FEL, in bruikleen aan Ir. C.J. den Hollander
47. Archief TNO-FEL, in bruikleen aan Ir. V.F. Schenkelaars
48. Archief TNO-FEL, in bruikleen aan G.D. Klein Baltink
49. Archief TNO-FEL, in bruikleen aan Drs. E. van Halsema
50. Archief TNO-FEL, in bruikleen aan Drs. J.K. Vink
51. Archief TNO-FEL, in bruikleen aan Ing. D. Kloet
52. Archief TNO-FEL, in bruikleen aan Drs. J.S. Groot
53. Documentatie TNO-FEL
54. Reserve

Indien binnen de krijgsmacht extra exemplaren van dit rapport worden gewenst door personen of instanties die niet op de verzendlijst voorkomen, dan dienen deze aangevraagd te worden bij het betreffende Hoofd Wetenschappelijk Onderzoek of, indien het een K-opdracht betreft, bij de Directeur Wetenschappelijk Onderzoek en Ontwikkeling.

\* Beperkt rapport (titelblad, managementuittreksel, RDP en distributielijst).